BBA - Molecular Cell Research 1872 (2025) 119865

Contents lists available at ScienceDirect

BBA - Molecular Cell Research

journal homepage: www.elsevier.com/locate/bbamcr

Review

Synergy of native mass spectrometry and other biophysical techniques in studies of iron-sulfur cluster proteins and their assembly

Jason C. Crack, Nick E. Le Brun *

School of Chemistry, Pharmacy and Pharmacology, University of East Anglia, Norwich Research Park, Norwich NR4 7TJ, UK.

ARTICLE INFO

Keywords:
iron-sulfur cluster
Mass spectrometry
DNA regulation
Iron sensing
O_2 sensing
Nitric oxide sensing
iron-sulfur cluster biogenesis

ABSTRACT

The application of mass spectrometric methodologies has revolutionised biological chemistry, from identification through to structural and conformational studies of proteins and other macromolecules. Native mass spectrometry (MS), in which proteins retain their native structure, is a rapidly growing field. This is particularly the case for studies of metalloproteins, where non-covalently bound cofactors remain bound following ionisation. Such metalloproteins include those that contain an iron-sulfur (Fe—S) cluster and, despite their fragility and O_2 sensitivity, they have been a particular focus for applications of native MS because of its capacity to accurately monitor mass changes that reveal chemical changes at the cluster. Here we review recent advances in these applications of native MS, which, together with data from more traditionally applied biophysical methods, have yielded a remarkable breadth of information about the Fe—S species present, and provided key mechanistic insight not only for Fe—S cluster proteins themselves, but also their assembly.

1. Introduction

Iron-sulfur (Fe—S) clusters are defined as complexes of iron (Fe^{2+} or Fe^{3+}) and sulfide (S^{2-}) ions, of variable nuclearity. Their significance stems from their widespread distribution throughout life, where they fulfil a myriad of functions as co-factors of proteins [1–3]. They are conjectured to be the most ancient of all protein co-factors, evolving prior to photosynthesis in an anaerobic world in which soluble iron (as Fe^{2+}) and sulfur (as S^{2-}) were abundant. Indeed, some have speculated that chemistry involving Fe—S species may have played a central role in the origin of life [4].

1.1. Structure and properties of iron-sulfur clusters

The two most common Fe—S clusters in biology are the [2Fe—2S] and [4Fe-4S] clusters. The [2Fe—2S] cluster is the simplest of Fe—S clusters, consisting of a $[Fe_2(\mu_2\text{-}S)_2]$ unit arranged as a rhomb, where the two iron ions are coordinated by two additional ligands from the protein, Fig. 1, in the form of the side chains of certain residues. The thiolate (RS^-) side chain of cysteine most commonly serves this role, but other residues are occasionally found to serve as cluster ligands, including aspartate/glutamate ($RCOO^-$), histidine (-N=) and serine (RO^-) [5–8]. The [4Fe—4S] cluster is a cuboid consisting of two interlaced tetrahedra of irons and sulfides (Fig. 1), with each iron coordinated by one other ligand. Again, for protein-bound clusters, this is commonly a cysteine thiolate, but, as for [2Fe—2S] clusters, other amino acid residues sometimes serve as ligands, and in some cases a non-protein ligand is found [6,8]. The [3Fe—4S] cluster, which equates to a [4Fe—4S] cluster lacking an iron at one of its vertices, is found in a limited number of cases.

The different geometric arrangements and protein coordination of [2Fe-2S] and [4Fe-4S] clusters have important consequences for the protein environment surrounding the cluster. In all cases, the irons are tetrahedral; for [2Fe—2S] clusters, two of the four ligands to each iron are provided by the protein and are perpendicular to the $[Fe_2(\mu_2\text{-}S)_2]$ rhomb. Thus, the protein ligands all lie in the same plane. Conversely, for [4Fe—4S] clusters, only one (or up to one) of the four ligands to each iron is provided by the protein, and so these are in a tetrahedral arrangement, echoing the arrangement of the irons themselves. The important point, here, is that while four amino acid side chains (typically) coordinate both [2Fe-2S] and [4Fe-4S] clusters, the arrangement of those ligands is very different, and so the type of cluster bound has important structural consequences for the protein. Thus, an Fe-S-binding motif may be capable of binding either a [4Fe—4S] or a [2Fe—2S] cluster, but it cannot switch between cluster types without a change in protein conformation. In addition to the above Fe—S clusters, more

* Corresponding author.
E-mail address: n.le-brun@uea.ac.uk (N.E. Le Brun).

https://doi.org/10.1016/j.bbamcr.2024.119865
Received 16 February 2024; Received in revised form 5 July 2024; Accepted 10 October 2024
Available online 21 October 2024

exotic iron- and sulfide-containing clusters exist, but we will not consider those further here.

Fe—S clusters exhibit complex electronic and magnetic properties, involving electron delocalization and the sulfide bridge-mediated coupling of spins on different iron ions. A result of this is that clusters can be found in a limited number of charged states, with the protein environment typically limiting it to, usually, two oxidation states. The +2/+1 states of both [2Fe-2S] and [4Fe-4S] clusters are most common for electron transfer proteins [8], though the latter also sometime operate over the +3/+2 couple [10]. Observation of a single oxidation state clearly indicates a function other than electron transfer for the cluster. UV–visible absorbance spectra are dominated by transitions due to ligand to metal charge transfer, resulting in distinct (oxidation state-dependent) spectra for [2Fe—2S] and [4Fe-4S]. Absorbance intensity of [2Fe-2S] clusters extend further into the visible than that for [4Fe—4S], resulting in a red-brown colour, while those of [4Fe-4S] clusters are straw brown, darkening to green-brown in highly concentrated solutions [11].

Magnetic coupling of the spins of paramagnetic iron ions very often results in diamagnetic (S = 0) or low value (S = ½) spin states [8,12–14] giving electron paramagnetic resonance and Mössbauer spectra that are typically highly characteristic of the cluster type [15,16]. Other spectroscopic methods can also provide information on cluster type and, in some cases, coordination. Resonance Raman, for example, reports cluster-specific vibrations that give information on the cluster type as well as coordinating ligands [17]. Nuclear resonance vibrational spectroscopy (NRVS) also provides vibrational information that is specific to the cluster iron and its coordination [18]. All of these methods have proved to be very useful in studies of Fe—S cluster proteins. In general, all involve measurements of highly concentrated samples in the frozen state, and, in the case of Mössbauer and NRVS, ^{57}Fe-labelling of the clusters. Thus, these methods do not readily lend themselves to kinetic measurements of reactions involving Fe—S clusters.

1.2. Biological functions of protein-associated iron-sulfur clusters

Fe—S clusters perform essential functions in a wide variety of processes, including respiration, photosynthesis, and nucleic acid metabolism [19]. The first Fe—S cluster proteins discovered, in the 1960s, were ferredoxins that function in electron transfer. While this is a key role, several other functions of Fe—S clusters have since been discovered, including as catalysts of both non-redox reactions and redox reactions. In the former, the cluster acts as a Lewis acid, e.g. in aconitase, [20]. In the latter, reactions that involve electron transfer in addition to chemical transformations are catalysed by, e.g., radical SAM enzymes. Here, the cluster participates in radical chemistry to facilitate methylation and other transformations [21]). There are some examples of enzymes, such as biotin synthase and lipoic acid synthase, in which an Fe—S cluster functions to provide sulfur for a biosynthetic process [22]. Besides catalysis, there are an increasing number of Fe—S cluster proteins that function in gene regulation. Here, the cluster functions as a sensor for one or more key environmental molecules that signal, for example, nutritional or redox status or stress (oxidative or nitrosative) [23].

1.3. Reactivity of protein-associated iron-sulfur clusters

The evolution of Fe—S clusters occurred in an anaerobic world in which iron and sulfur were plentiful. The oxygenation of the atmosphere presented a huge challenge in that Fe—S clusters are in general inherently chemically reactive, and highly susceptible to damage under aerobic conditions as a result of reaction with O_2. In addition to this, following oxygenation, both iron and sulfur became much less bioavailable due to oxidation; in particular, the most stable form of iron under aerobic/aqueous conditions, Fe^{3+}, is highly insoluble. That Fe—S clusters were not 'abandoned' as cofactors during evolution is a testament to their unique properties/capabilities, which could not (at least broadly) be easily replaced by more bioavailable and robust alternatives.

Under conditions of aerobic respiration, which are not generally considered particularly 'stressful', the demand for Fe—S clusters in bacteria is significantly higher than under anaerobic or micro-aerobic conditions [24], reflecting their reactivity with O_2. Fe—S cluster biogenesis machineries, such as SUF, evolved to ensure that cluster supply could be met under aerobic conditions, and even under iron limitation and/or conditions of oxidative stress [25].

The reactivity of Fe—S clusters has also been exploited during evolution to enable organisms to sense their environments, from various stresses to nutritional status. For example, in many bacteria, the presence/absence of O_2 is sensed by an Fe—S cluster-containing regulatory protein, FNR, where direct reaction of O_2 with the cluster is the basis of the sensing reaction [26]. Another key sensing reaction occurs between Fe—S clusters and nitric oxide, an indicator of nitrosative stress. Again, in many bacteria, NO is sensed by an Fe—S cluster regulator, e.g. NsrR [27]. In these cases, where the cluster functions as a sensor, reaction at the cluster results in transduction of the signal to effect a protein conformational change that is triggered by a rearrangement of Fe—S cluster ligand residues. This, in turn, affects the interaction of the regulatory protein with its cognate partner, which for bacterial regulators, is a specific DNA operator sequence. For higher eukaryotes, including

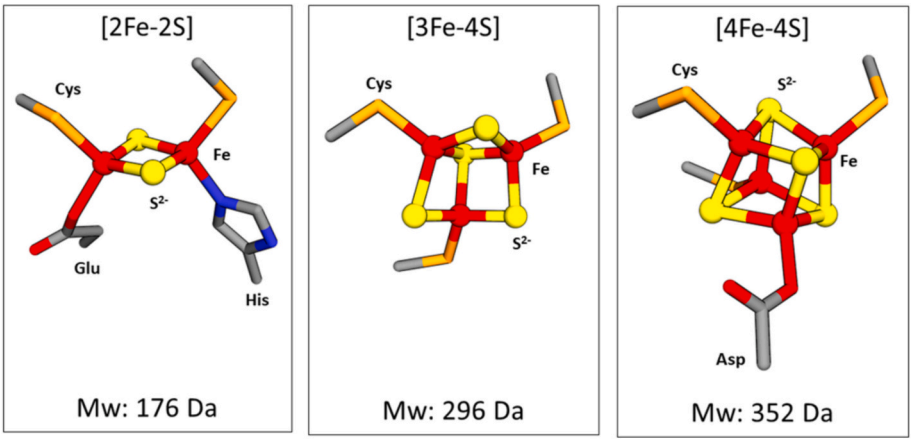

Fig. 1. Commonly found protein-associated iron-sulfur clusters. Structures of [2Fe-2S], [3Fe—4S] and [4Fe-4S] iron-sulfur clusters (PDB: 6HSD, 2VKR, 5N07). Iron, sulfide and ligands (Cys, Asp, His, and Glu residues) are indicated, along with the mass of the cluster. Structural images in this review were produced using UCSF ChimeraX [9] or Discovery studio (Dassualt Systèms Biovia Corp).

humans, the cognate partner may be mRNA (e.g. IRP1 [28]). FNR and NsrR, as well as other examples of Fe—S cluster regulators, are discussed in detail in this review.

1.4. Mass spectrometry of iron-sulfur cluster proteins

Electrospray ionisation (ESI) and matrix-assisted laser desorption ionisation (MALDI) are widely applied to studies of macromolecules because they are soft ionisation sources that do not impart high energies to analyte molecules and thus do not result in significant fragmentation. ESI is distinct in that it does not require addition of a matrix or drying of samples and is carried out on samples in solution. Most applications of ESI involve acidic solvents that preserve sample molecules intact but not their native structure. However, by selecting aqueous, volatile buffer systems at or close to neutral pH for studies of biologically relevant samples, it is possible to do both and thus to gain additional information about structure or the formation of complexes of different types.

The above approach is often described as 'native MS' and we will use this term here; the literature contains an array of alternative terminology (e.g. native spray, non-covalent, non-denaturing, macromolecular or supra-molecular) that describes the same basic approach to ESI-MS in which non-covalent interactions are preserved [29,30]. Improvements in instrument resolution and sensitivity mean that native MS is now commonly applied for accurate mass determination of proteins, protein complexes, and studies of interactions of proteins with small molecules, lipids, sugars and nucleic acids, as well as protein structural changes [31–37].

ESI-MS of metalloproteins (encompassing 'native' as well as more traditional approaches but where the metal remained bound) has in some cases provided valuable insight into the metal centre [38–49]. Due to their reactivity, Fe—S cluster proteins have been generally more difficult to study by ESI-MS. Fe—S clusters are unstable at low pH and were degraded under the acidic conditions of early ESI-MS experiments. Some early successes using aqueous buffers were generally confined to the most stable Fe—S proteins; for example, the high potential iron-sulfur protein (HiPIP) from *Chromatium tepidum* exhibited three distinct charge states (+5 to +7) corresponding to the [4Fe—4S] cluster-bound form, indicating the experimental conditions were sufficiently mild so as to preserve the fragile Fe—S bonds [50]. The generally good stability of ferredoxins of both [2Fe-2S] and [4Fe-4S] cluster types, particularly around neutral pH, meant that they were ideal protein systems for the establishing a set of conditions for the investigation of other, less stable Fe—S cluster proteins [51], and they continued to be useful test subjects when exploring the capabilities of more modern ESI-MS instruments [52–54].

More recently, further advances in instrument sensitivity and resolving power together with improved methods for handing highly sensitive Fe—S cluster proteins have led to applications of native MS to a wider range of Fe—S proteins, and particularly those that function as regulatory proteins. In part, this is because the clusters of such proteins undergo chemical reactions at their clusters as part of their sensing mechanisms, resulting in mass changes. While methods such as Mössbauer, resonance Raman and electron paramagnetic resonance (EPR) spectroscopies can provide key information about the nature of Fe—S clusters, they have more limited capacity to elucidate Fe—S cluster reaction mechanisms. As illustrated in this review, native MS is extremely powerful in this regard, because it can simultaneously follow all species (original cluster, cluster products and intermediates).

1.4.1. Practical considerations for native mass spectrometry of iron-sulfur cluster proteins

It is useful here to outline some of the practical considerations when conducting native MS studies of Fe—S cluster proteins. Firstly, it is worthwhile to direct effort into optimising over-expression conditions to maximise in vivo cluster incorporation [55,56]. Isolation of the protein should also be optimised to achieve the highest possible purity, and resulting samples analysed by standard LC-MS to confirm the absence of contaminants and to verify that the mass of the apo protein matches that predicted [57].

In some cases, isolated proteins exhibit low cluster loading. Indeed, it is the case that some Fe—S proteins, particularly those expressed heterologously in *E. coli*, appear to be poor clients for the native Isc/Suf Fe—S assembly machineries, or are so reactive that only apo proteins are obtained [55,58]. In such cases, in vitro methods of cluster insertion can be used to achieve satisfactory cluster incorporation. Two principal methods are available: first, a semi-biomimetic approach that employs a cysteine desulfurase (e.g. NifS, IscS) to generate in situ sulfide ions from cysteine substrate; second is a purely chemical approach that involves the addition of S^{2-} ions (as Na_2S or Li_2S) to the apo-protein solution. Both approaches also involve addition of Fe^{2+}/Fe^{3+} ions (as $(NH_4)_2Fe(SO_4)_2$ or $FeCl_3$, respectively) and reductant (commonly DTT) [55,59]. In most cases, in vitro cluster reconstitutions can faithfully assemble the native Fe—S cluster, but caution should be exercised, because erroneous results are possible [60]. Spectroscopic properties should, where possible, be compared to the Fe—S cluster(s) inserted by in vivo systems [55]. Furthermore, it's important to keep chemical artefacts (such as adventitiously bound Fe/S species) to a minimum.

Prior to performing native MS all non-volatile salts and buffer components must be removed from samples and substituted with volatile 'buffer' components [57,61,62]. Solutions of ammonium acetate are commonly employed for native MS, but other volatiles, such as ammonium formate, may also be used [57,61–65]. Failure to remove non-volatiles results in poor ionisation. The buffer conditions often have to be optimised in order to maximise ionisation for native MS studies; as a starting point, we typically use 250 mM ammonium acetate, pH 8.0, and adjust from there [57]. Ionisation efficiency is not uniform, and the presence of readily ionisable contaminants can lead to suppression of analyte ionisation; thus, it is very important that the sample is as pure as possible and thoroughly exchanged into the appropriate volatile buffer.

Ionisation can usually be further optimised by 'tuning' instrument parameters [57]. For example, with an instrument equipped with an ESI source and a Time of Flight (TOF) mass analyser (Fig. 2), the source, ion transfer, and TOF parameters can all be adjusted to maximise signal intensity and resolving power, while also keeping to a minimum any damage to the Fe—S cluster(s) or protein-protein interactions due to in-source or collisional damage [57,61,62].

1.4.2. Interpretation of mass spectrometry data for iron-sulfur cluster proteins

Ions entering the mass analyser are not resolved according to their mass, but rather their mass-to-charge ratio (m/z). Time-of-flight properties for an ion is proportional to the square root of the mass of the ion; thus, ions of lower m/z value reach the detector sooner than higher m/z value ions (of greater mass if charge is the same). For a TOF-equipped instrument, the time elapsed between the acceleration pulse and ion detection (t) is measured and, along with acceleration voltage (V) and length of the drift region (d), is used to determine the m/z value of the detected ion(s) according to:

$$m/z = 2eV\left(\frac{t^2}{d^2}\right) \quad (1)$$

where m is the mass of the ion, z is the number of charges on the ion and e is the electron charge. In general, when compared to denatured/unfolded proteins, folded proteins have comparably fewer residues that are readily accessible to the ion generation process. Thus, when native MS and LC-MS spectra for the same protein are compared, the former typically exhibit few charge states with lower total charge values. In some cases, the native MS spectrum might reveal a mix of charge state envelopes due to folded and (partially) unfolded conformations, reflecting the same above characteristics.

Protein mass can be readily calculated from the m/z spectrum,

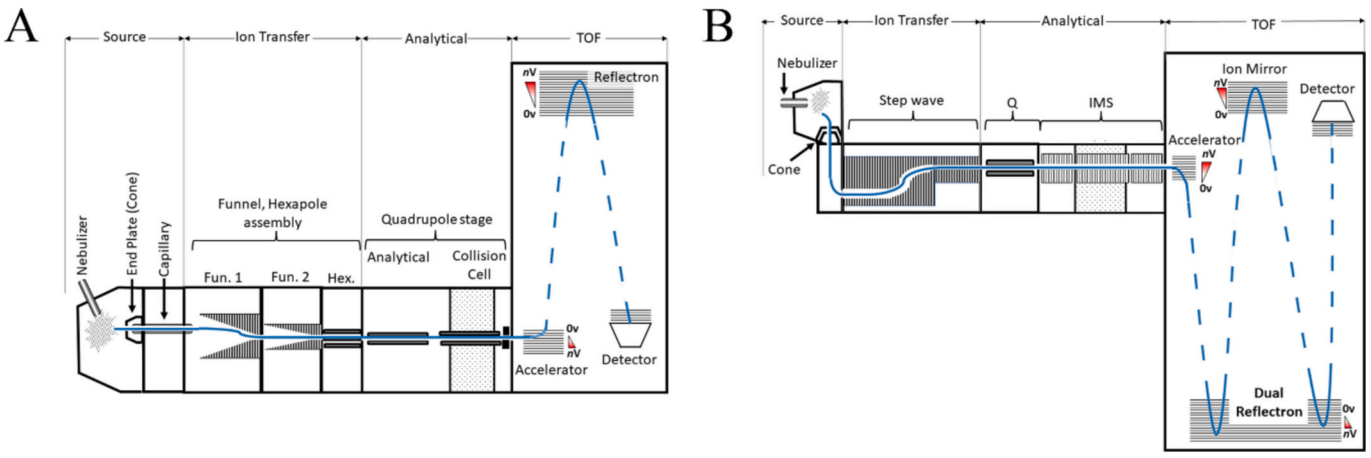

Fig. 2. Schematic representation of a Q-TOF mass spectrometer. Schematic representation of a A) a typical micro-Q-TOF and B) a newer hybrid Q-TOF featuring ion mobility spectroscopy (IMS) capability. The mass spectrometer consists of four essential components that function in ionisation (e.g the source), ion transfer (e.g. funnel or step-wave), analysis which is coupled to the TOF stage (e.g. dual quadrupole arrangement or quadrupole-ion mobility stage, in A) and B) respectively), and detection (located in the TOF stage). Collision induced dissociation (CID) typically occurs in the source (isCID) via the cone or the analytical stage via a dedicated collision cell (shown in A), or as part of the IMS region (shown in B). The blue line represents the path taken by ions through the instrument. The field-free drift region (s) are indicated by a dashed blue line. Both types of mass spectrometer are capable of native MS, and have been used in some of the studies mentioned in the proceeding sections. (For interpretation of the references to colour in this figure legend, the reader is referred to the web version of this article.)

particularly if all the charge on the ion (generated by positive mode ESI) results from an excess of protons (or a deficit of protons in negative mode). For apo proteins (via LC-MS or native MS), these masses are determined from the *m/z* spectrum according to:

$$m/_z = [M + zH] \Big/ z \tag{2}$$

where M is the molecular mass of the protein, H is the mass of the proton and *z* is the charge of the ion. The analysis of metalloproteins is more complex because the metal containing cofactors are themselves usually charged, and thus contribute to the overall ion charge; thus, not all of the charge is derived from additional protons, and the charge of the cofactor must be considered in order to accurately determine the mass from the *m/z* spectrum.

For an Fe—S cluster protein, the peaks correspond to:

$$m/_z = [M + [FeS]^x + (z - x)H] \Big/ z \tag{3}$$

where *M* is the molecular mass of the protein, [Fe—S] is the mass of the iron sulfur cluster with *x* charge, *H* is the mass of the proton and *z* is the charge of the ion. In this equation, the charge of the cluster (*x*), decreases the number of protons required to obtain an ion with *z* charges. Post deconvolution (e.g. using Unidec, [66]), the observed neutral mass is usually off-set from the predicted mass by a mass equivalent to the charge of the cluster:

$$M^{obs} = [M + ([FeS] - x)] \tag{4}$$

For example, if a protein with mass *M* binds a $[2Fe—2S]^{2+}$ cluster, the relevant peak (M^{obs}) in the deconvoluted neutral mass spectrum for the holo protein will be observed at:

$$M^{obs} = (M + (176 - 2)) \tag{5}$$

The same principle applies to $[4Fe\text{-}4S]^{2+}$ clusters and any cluster intermediates [47,54,67].

Identifying the origin of signals in the mass spectrum may not be straightforward. Usually, this is not done based only on MS data; data from spectroscopic and other bioanalytical techniques are used to inform assignment. Even then, it may be hard to distinguish between species of similar mass. In such cases, stable isotope substitution data are crucial for unambiguous confirmation of the assignment of peaks to particular reactants, intermediates, and products. We have previously described a general set of conditions that are suitable for the preparation of isotopically enriched (>99 %) Fe—S clusters from ^{34}S, ^{57}Fe or $^{34}S/^{57}Fe$ [56,67–70]. With such enriched samples, the differences between natural abundance and enriched sample MS spectra reveal the identity of the species. For example, a mass difference of ~ + 8 Da (natural abundance versus ^{34}S enriched) is expected for a [4Fe—4S] cluster, in which each sulfide has a mass offset by +2 Da in the enriched sample. Reactions with NO (mass of 30 Da), resulting in cluster nitrosylation may be particularly problematic in terms of assignment, because a gain of one NO molecules is difficult to distinguish from gain of two NO and a loss of one sulfide. Use of ^{15}NO and/or ^{34}S enrichment permits unambiguous assignment [68,71].

Here, we summarise recent advances in the application of native MS in studies of Fe—S cluster proteins, including several regulators, and the scaffold protein of the Isc Fe—S biogenesis machinery. These studies demonstrate the capacity of this approach to provide novel insight that cannot be easily otherwise obtained.

2. Native MS as a tool for determining Fe—S cluster type

2.1. Common spectroscopic methods for determining Fe—S cluster type

Whether or not an Fe—S cluster is present in a purified protein sample can be quickly assessed using little more than an absorbance spectrophotometer. Spectra of [4Fe-4S] and [2Fe-2S] clusters are generally distinct in appearance, and can provide an indication of cluster type [59,72]. However, the broad and overlapping bands, as well as dependence on (variable) coordinating ligands, means that absorbance spectra alone do not provide conclusive evidence.

The asymmetric fold of the protein generally confers optical activity on Fe—S cluster electronic transitions, resulting in a circular dichroism (CD) band pattern that is characteristic of the cluster and its environment. While the CD pattern of related Fe—S proteins is usually similar (e.g. Section 3.3), the CD pattern alone may not be useful in identifying cluster type [73,74]. Other techniques, such as magnetic CD (MCD), resonance Raman, nuclear vibrational resonance (NRVS), Mössbauer and EPR spectroscopies are useful to establish cluster type (see Section 1.1). A combination of two or more such methods typically provides unambiguous assignment.

2.2. Determining Fe—S cluster type using native MS alongside other biophysical methods

Native MS can now be added to (near or at the top of) this list of techniques. In comparison to spectroscopic techniques mentioned, native MS is significantly less demanding in terms of sample ($\leq$ 20 μM), can be applied without isotopic enrichment (at least for cluster identification), and can resolve all Fe—S cluster species present in the sample, irrespective of oxidation state, in one experiment. For this reason, native MS is routinely used in our lab, alongside spectroscopic methods, to determine the nature of clusters present in Fe—S proteins.

2.2.1. S. venezuelae RsrR

Native MS has been commonly applied in studies of clusters bound to members of the Rrf2 superfamily of bacterial transcriptional regulators [75,76]. For example, although the *S. venezuelae* protein Sven6563 (RsrR) was originally proposed to be a homolog of NsrR, anaerobic preparations of RsrR revealed quite different optical properties, with a weak pink colour [77] (Fig. 3A). The initial native mass spectrum revealed both monomeric and dimeric forms of the protein (Fig. 3B), reflecting the well-known phenomenon of partial dissociation of dimeric proteins in the gas phase [67,78,79]. In most cases, this has proved advantageous because of the resulting simplification of peak assignments, where possible ambiguity arising from the presence of two subunits that might contain different Fe—S species is avoided.

In the monomeric region, a peak at 17,363 Da together with a notable peak at +176 Da corresponded to the presence of apo RsrR and [2Fe-2S] RsrR, respectively (Fig. 3C). The dimer region contained a peak at 34,726 Da that corresponded to the presence of apo RsrR homodimer. Two additional peaks at +176 and + 352 Da indicated the presence of a dimer with one [2Fe—2S] and two [2Fe-2S] clusters (or potentially a dimer with one [4Fe—4S] cluster), respectively (Fig. 3D). The absence of a [4Fe—4S] cluster peak (at +352 Da) in the monomer region strongly indicated that RsrR dimers contain one [2Fe—2S] per monomer, consistent with the subsequent crystal structure of RsrR (Fig. 3B, inset) [6,77]. This revealed asymmetric coordination of each [2Fe-2S] cluster at the monomer-monomer interface, involving two Cys residues from one subunit and His and Glu residues from the other (see [2Fe—2S] in Fig. 1). This was the first example of cluster coordination involving three different types of amino acid side chains [6].

Having established that RsrR harbours a [2Fe—2S] cluster with unique coordination, it was demonstrated that binding of RsrR to promoter sequences is modulated by the redox status of the [2Fe—2S] cluster. Through a combination of chemical modification/LC-MS, site-directed mutagenesis, X-ray crystallography and computational studies, it was shown that upon reduction of the $[2Fe—2S]^{2+}$ cluster to the $[2Fe—2S]^{+}$ form, Trp9 undergoes a 100° rotation into a cavity that is created upon protonation of His33 (close to the cluster, but not coordinating). The resulting conformational change in the DNA-binding domain abolishes DNA binding [6,80]. Given the above observations, Sven6563 was named RsrR, for Redox sensitive response Regulator [6,77,80].

2.2.2. Nuclear receptor coactivator 4 (NCOA4) protein

A further example of native MS being used to determine cluster type, concerns the enigmatic nuclear receptor coactivator 4 (NCOA4) protein. Proteomic studies identified NCOA4 as a facilitating factor involved in the degradation of ferritin, and concomitant release of Fe ions to the cytosol [81,82]. Kuno et al [83], found that NCOA4 assists in the delivery of ferritin molecules to the lysosome and that the O_2 level determines the fate of ferritin in an NCOA4-dependent manner. When purified, NCOA4 exhibited spectroscopic properties consistent with an Fe—S cluster cofactor, which under O_2-limiting conditions made NCOA4 susceptible to degradation by HERC2, and no longer capable of facilitating ferritin degradation [83,84]. Recently, Zhao et al showed that the C-terminal, cysteine-rich ferritin-binding domain of NCOA4 binds an

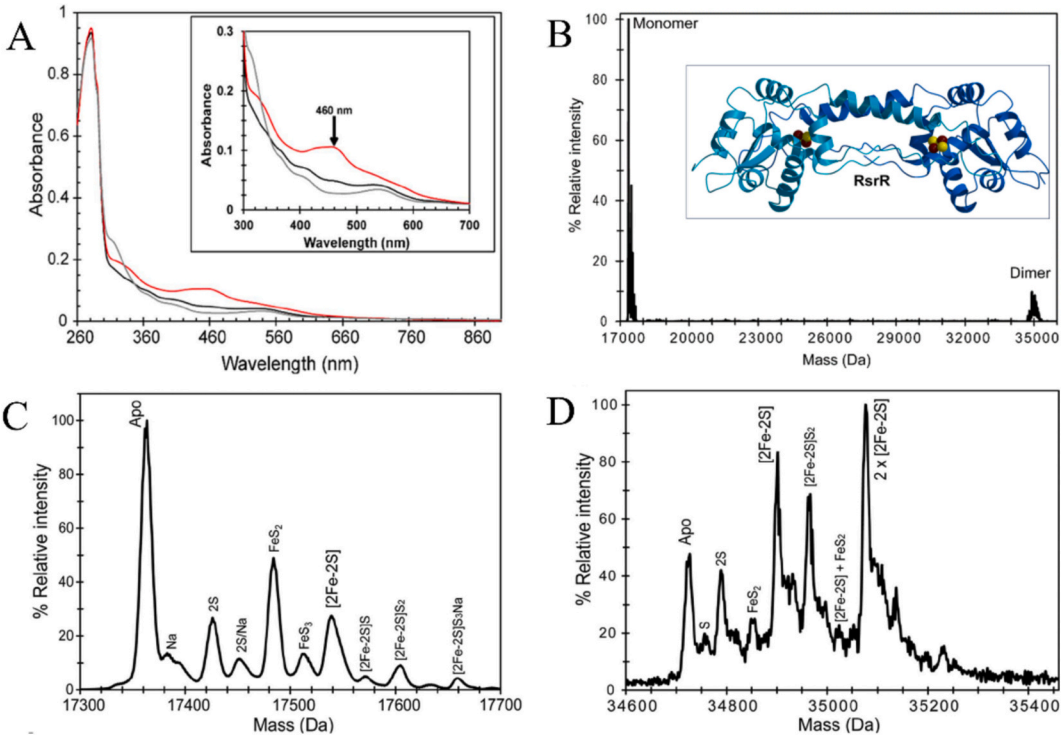

Fig. 3. Characterisation of RsrR. A) Absorption spectrum of [2Fe-2S] RsrR as isolated 'pink' form (black line), oxidised (red line) and reduced (grey line); inset is the absorption spectrum in more detail. λ_{max} for the oxidised form is indicated. B) Full range native deconvoluted MS spectrum of RsrR indicates the presence of dimeric and monomeric forms of RsrR; inset shows subsequent crystal structure of RsrR (PDB: 6HSD) [6]. C) and D) show the monomeric and dimeric regions of the mass spectrum in more detail. The data indicate one [2Fe—2S] cluster per monomer, consistent with structural observations [6,77]. (For interpretation of the references to colour in this figure legend, the reader is referred to the web version of this article.)

Fe—S cluster with spectroscopic and native MS properties consistent with the presence of a [3Fe—4S] cluster. Although NCOA4 is naturally multimeric, the process of ionisation resulted, as above, in the separation of NCOA4 into monomers, simplifying the assignment of associated Fe—S species. Thus, under iron limitation, Fe—S cluster assembly becomes deficient and NCOA4 fails to acquire a cluster, inhibiting NCOA4 degradation by HERC2 [84,85]. The improved stability of NCOA4 then facilitates the targeting of ferritin to the lysosome and its subsequent degradation, resulting in release of Fe ions. The increase of available iron restores Fe—S cluster assembly such that NCOA4 is again susceptible to HERC2-mediated degradation [85].

2.2.3. *The FixABCX protein complex of A. vinelandii*

A further example of the application of native MS is studies of the FixABCX protein complex of *A. vinelandii*, which bifurcates electrons derived from NADH towards the nitrogenase enzyme or other cellular processes. FixABCX is a multi-cofactor protein complex, binding multiple molecules of FAD, in addition to Fe—S clusters. FixA, FixB and FixC are each predicted to bind a single FAD molecule, while the Fe—S clusters are associated with FixX. Native MS in combination with spectroscopic techniques was utilised to characterise the FixABCX complex [86]. During ionisation, the FixABCX complex dissociated to give distinct FixAB and FixCX sub-complexes. FixAB had a molecular mass of 71,415 Da (determined from the deconvoluted neutral mass spectrum), corresponding to the predicted mass of FixAB with two bound FAD molecules (predicted mass 71,414 Da). The FixCX sub-complex had a molecular mass of 60,310 Da, which is slightly greater than predicted for FixCX with a bound FAD and two [4Fe-4S] clusters, 59,933 Da. It was noted that the difference in mass, +377 Da, is close to the expected mass of riboflavin, suggesting that this cofactor may be associated with the complex. From these, and other observations, it was shown that electrons derived from NADH arrive on the FAD cofactor of FixA, where bifurcation occurs: the first electron arriving on FixA is diverted to towards the FAD cofactors of FixBC, while subsequent electrons are directed to the [4Fe—4S] clusters of FixX, and are destined for nitrogenase only when electrons accumulate on FAD cofactors of FixCD prior to transfer to coenzyme Q [86].

Overall, the studies highlighted in Section 2 show the power of native MS to identify the nature of the cluster(s) associated with a particular protein. This approach is particularly powerful when combined with spectroscopic methods, e.g. EPR, Mössbauer, resonance Raman or MCD.

3. Native MS of Fe—S cluster-containing regulatory proteins

As illustrated in Section 2, native MS uniquely provides accurate mass measurements of species in which non-covalent interactions are preserved. Native MS can also report on intermediate species in both thermodynamic and kinetic experiments. Here, we provide selected examples where native MS has been used to follow cluster conversion, allowing for the elucidation of molecular events. It has also been used to probe protein-protein interactions and study the process of Fe—S cluster assembly.

3.1. *O_2 sensing by Fe—S cluster proteins: FNR, a master regulator of the aerobic-anaerobic respiratory switch*

Among the best studied Fe—S cluster regulators is the Fumarate and Nitrate Reduction (FNR) regulator from *E. coli,* which belongs to the larger CRP/FNR protein family of dimeric transcriptional regulators. These function in sensing important environmental changes, such as gaseous signalling molecules (e.g, O_2, NO, CO), redox balance, or nutrient availability (e.g cAMP) [87–92]. Prior to work on FNR, [4Fe—4S] to [2Fe-2S] cluster conversions typically required the presence of chelators, detergents, or other non-physiological reagents [93]. In the case of *E. coli* FNR, studies employing Mössbauer spectroscopy showed that FNR acquired a [4Fe—4S] cluster under anaerobic conditions, and that it undergoes conversion to a [2Fe—2S] cluster in response to dissolved O_2, with an accompanying loss of DNA binding [94,95].

The presence of the [4Fe—4S] cluster is intimately connected to FNR function, as it promotes a conformational arrangement that minimises inter-subunit charge repulsion that otherwise render FNR a monomer. The resulting [4Fe—4S] FNR dimer binds DNA site-specifically, and, in some cases, contacts the transcriptional machinery leading to activation [96,97]. The process of cluster conversion is not simple, as indicated by discovery of a $[3Fe—4S]^{1+}$ intermediate (Fig. 4A), and persulfide-coordinated [2Fe-2S] forms (Fig. 4B) [17,55,97–99]. Structural characterisation of FNR, as for many O_2-sensitive Fe—S cluster proteins proved to be extremely challenging. This was eventually achieved in 2015 through the crystal structure of *Allivibrio fischeri* (Af) [4Fe—4S] FNR (87 % identity to *E. coli* FNR) [100]. Prior to this, models based on the structure of CRP and a series of *E. coli* FNR mutants that exhibited significant differences in cluster stability (and thus gene regulation) when exposed to O_2 were the basis for understanding the role of the [4Fe—4S] cluster in controlling FNR function [101]. Substitution of Leu28 with His (L28H), or Ser24 with Phe (S24F) was subsequently found to improve the tolerance of the [4Fe—4S] cluster towards O_2, with L28H > S24F > wild type FNR (wtFNR) [102,103].

3.1.1. *Understanding cluster conversion and O_2 sensing through native MS and spectroscopic methods*

To gain further insights in the hidden complexity of O_2-mediated cluster conversion, we turned to native MS because of its ability to simultaneously resolve all Fe—S cluster species present in the sample irrespective of oxidation state or optical/vibrational properties. The S24F FNR variant was employed because it retains the same mechanism of conversion, via a $[3Fe—4S]^{1+}$ intermediate, as observed for wtFNR, but reacts more slowly with O_2 [104]. Thus, the properties of S24F are better suited to time-resolved native MS studies than the significantly faster reacting wtFNR [55,99,104]. L28H, by contrast, exhibits an even-greater O_2 resistance than S24F, meaning that intermediates of cluster conversion are not readily detectable [67,105].

Under anaerobic conditions the deconvoluted neutral mass spectrum in the dimeric region primarily featured [4Fe-4S] S24F FNR homo-dimer (59,796 Da), consistent with previous solution studies [106]. Exposure to O_2 resulted in low intensity peaks due to dimers containing at least one [3Fe—4S] cluster, indicating that cluster conversion coordinated dissociation into FNR monomers. The monomeric region of the spectrum, featuring [4Fe—4S] S24F FNR (29,898 Da), was used to greatly simplify cluster assignment (as explained in Section 2.2.1.). Reaction with O_2 yielded the previously reported [3Fe-4S], [2Fe—2S], and persulfide-coordinated forms of [2Fe-2S] S24F FNR, but also unveiled a previously unknown [3Fe-3S] intermediate, along with persulfide adducts of apo FNR [67] (Fig. 4C). A small molecule $[3Fe—3S]^{3+}$ cluster complex, in which the Fe and S ions are arranged in planar alternating ring structure, suggested that such an intermediate could be sufficiently stable to enable observation [107]. In fact, hints that such a species might exist within a protein environment were reported in an ESI Fourier transform ion cyclotron resonance MS study of *Pyrococcus furiosus* [3Fe-4S] FdI [54].

Kinetics of the O_2-mediated [4Fe-4S] S24F FNR cluster conversion reaction were established by time-resolved native MS. Signals associated with protein-bound cluster intermediates gained maximum intensity after ~15–30 min, while persulfide adducts of apo FNR continued to gain intensity up to ~30–50 min post O_2 exposure [67]. Global analysis of MS kinetic data showed that the first step of conversion involves the ejection of Fe^{2+} from the [4Fe—4S] cluster to form a [3Fe—4S] cluster (Fig. 4D), in line with previous spectroscopic studies. Although O_2 mediates the cluster conversion, initiated through the loss of an Fe^{2+}, it does not result in the formation of a stable O_2-derived complex. The details of this step are not entirely clear. The O_2 reaction could proceed

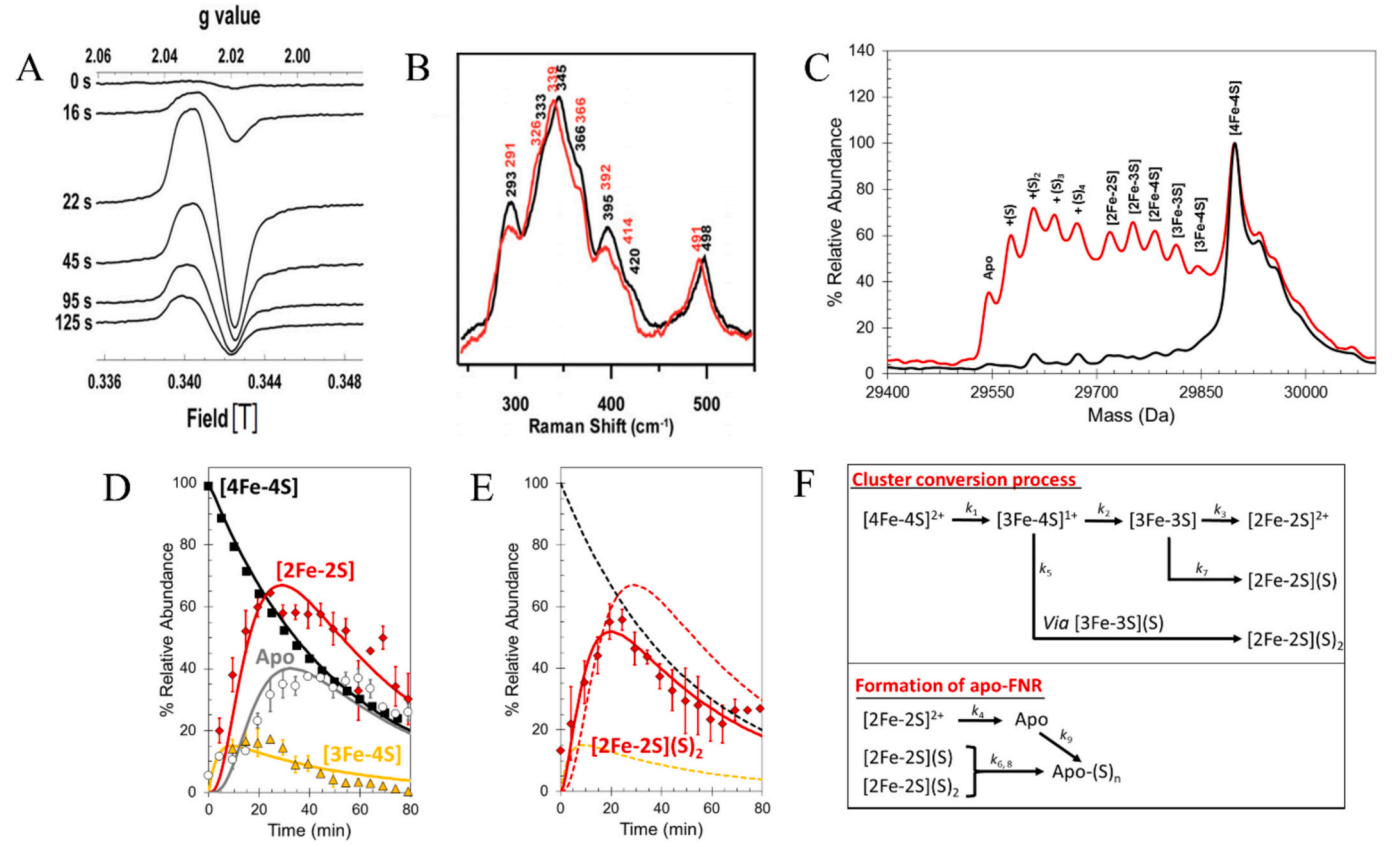

Fig. 4. Spectroscopic characterisation of [4Fe-4S] FNR reveals mechanism of cluster conversion. A) EPR spectra of FNR at increasing time after O_2 exposure reveal the presence of an $[3Fe\text{-}4S]^{1+}$ intermediate. B) Resonance Raman spectra of resulting [2Fe—2S] FNR with naturally abundant (black line) and ^{34}S enriched (red line) samples. The spectra indicate a persulfide ligated [2Fe-2S] cluster. C) Native MS of [4Fe-4S] S24F FNR before (black line) and after (red line) exposure to oxygen, results in the formation of several protein-bound clusters, as indicated. D) Relative abundances of [4Fe-4S] (black squares), [3Fe—4S] (yellow triangles), [2Fe—2S], apo (white circles) and E) [2Fe—4S] species as a function of time after O_2 exposure. Global fitting to the experimental data using the reaction scheme depicted in D) is shown in D and E by solid lines. Dashed lines in E show the response of [4Fe-4S], [3Fe—4S] and [2Fe-2S] clusters for easy comparison [17,67,99]. F) A summary of the FNR cluster conversion mechanism discussed here. (For interpretation of the references to colour in this figure legend, the reader is referred to the web version of this article.)

via direct oxidation of the cluster to an unstable $[4Fe\text{—}4S]^{3+}$ form from which Fe^{2+} ion is ejected, yielding the observed $[3Fe\text{-}4S]^{1+}$ species; alternatively, the Fe^{2+} might first dissociate, resulting in a $[3Fe\text{—}4S]^{0}$ cluster that is readily oxidised by O_2. We note that, in the crystal structure of [4Fe-4S] AfFNR, the electron density around Cys20 is substantially weaker than for the other cluster ligands (Cys23, 29, 122), differentiating this Cys20-Fe ion pair from the others of the cluster [100]. This could indicate that a weak interaction between Cys20 and the cluster facilitates a RirA-like $[4Fe\text{—}4S]^{2+} \longleftrightarrow [3Fe\text{—}4S]^{0} + Fe^{2+}$ equilibrium [67,70]. However, we note that, unlike RirA, the $[4Fe\text{—}4S]^{2+}$ of FNR is relatively insensitive to the presence of both Fe^{2+} and Fe^{3+} chelators [55], indicating that, if Fe^{2+} does dissociate as the first step, it is not accessible to non-physiological chelators.

The $[3Fe\text{—}4S]^{1+}$ intermediate is only transiently stable; loss of S^{2-} generates a [3Fe—3S] intermediate, the decay of which is the-rate limiting step in the overall $[3Fe\text{—}4S]^{1+}$ to $[2Fe\text{-}2S]^{2+}$ conversion process [67]. Adoption of a planar arrangement of the [3Fe—3S] cluster intermediate, as in the [3Fe—3S] small molecule complex, would provide a clear indication of how the tetrahedral array of Cys ligands to the [4Fe—4S] cluster transitions to a planar arrangement of the same ligands to the [2Fe—2S] form [67,107].

Both single and double persulfide-coordinated [2Fe-2S] species ([2Fe—2S](S) and $[2Fe\text{-}2S](S)_2$,respectively) were also observed, consistent resonance Raman spectroscopy. Importantly, kinetic data showed that these do not form after the [2Fe—2S] cluster (Fig. 4E) [17,67], but instead simultaneously with it, demonstrating that sulfide oxidation occurs at the same time as cluster conversion. Thus, the [3Fe—3S] cluster can degrade to generate both [2Fe-2S](S) and [2Fe-2S] clusters, and, similarly, the $[2Fe\text{—}2S](S)_2$ form is derived from the [3Fe—4S] cluster, possibly via a [3Fe—3S](S) intermediate. This indicates an oxidative branch of the main $[4Fe\text{-}4S]^{2+}$ to $[2Fe\text{-}2S]^{2+}$ cluster conversion pathway, rather than the incorporation of S^0 post-cluster conversion (Fig. 4F). As noted above (Section 1.4), $^{34}S/^{57}Fe$ isotope substitution data provided unambiguous confirmation of cluster species by native MS, and thus, the FNR mechanism summarised here [67].

3.1.2. *New structural insights into FNR cluster conversion*

The structure of [4Fe-4S] *Af*FNR revealed how the FeS cluster controls dimerization and also highlighted an unexpected link between the Fe—S cluster-binding domain and the ability of FNR to activate transcription (see [108,109]). Insights gained from the structure of [4Fe-4S] *Af*FNR have been correlated with existing substantial in vitro and in vivo data available for *E. coli* FNR [100,105,108,109]. The cluster-stabilizing effect of L28H and S24F substitutions, both located on the cluster-binding loop, favour Cys20 as the most likely candidate for initiating Fe loss in response to O_2. The recent crystal structure of L28H [4Fe-4S] *Af*FNR provides further valuable insights [105]. Here the L28H substitution leads to formation of a cation-π interaction between His28 and Arg184, which stabilizes the cluster-binding loop and hinders loop flexibility. A similar limitation of loop flexibility may also occur in S24F FNR. Loop flexibility and cluster reactivity appears to be intimately linked, and to be a crucial component of the outer sphere reaction of O_2

with the [4Fe—4S] cluster. Interestingly, loop flexibility appears to be less important for the inner sphere reaction of FNR with nitric oxide (NO), which is also physiologically relevant [110]. L28H FNR, which as mentioned is significantly affected in terms of its sensitivity to O_2 is largely unaffected in its reaction with NO, and, therefore, in comparison to wtFNR exhibits a greater relative specificity towards NO over O_2 [105].

3.2. NO sensing by Fe—S cluster proteins: NsrR, a regulator of nitrosative stress

The nitric oxide (NO)-sensitive repressor NsrR is found in most gram-

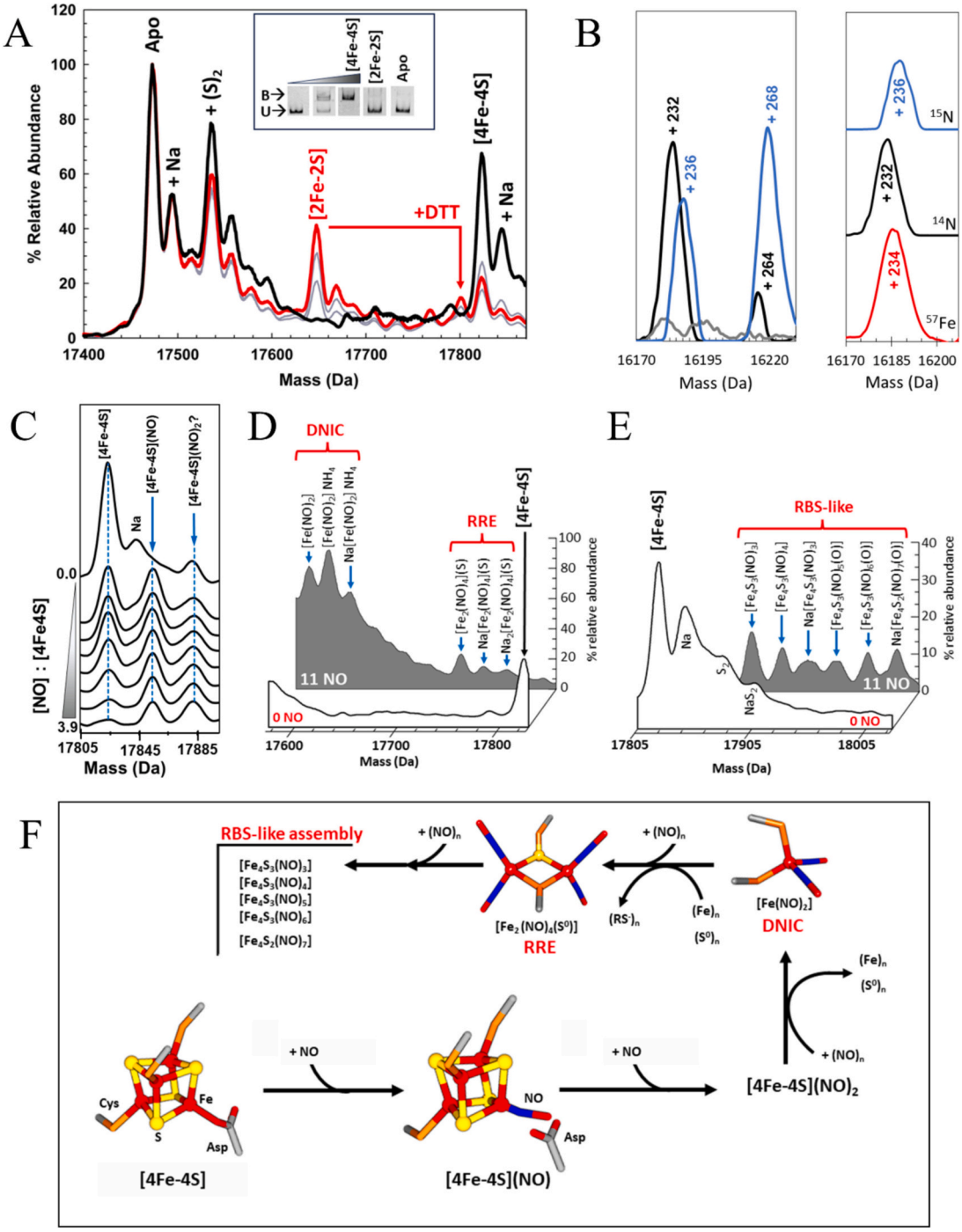

Fig. 5. Spectroscopic characterisation of [4Fe-4S] NsrR reveals mechanism of cluster nitrosylation. A) Native MS spectra of [4Fe-4S] NsrR with O_2 and DTT recorded at 0 min (black line); 15, 30, 45, 55 min (grey lines) and 65 min (red line) post exposure. Prior to the addition of DTT, no [2Fe-2S] clusters were observed. Inset, DNA-binding properties of forms of NsrR are shown. DNA containing the *hmpA1* promoter sequence was treated with [4Fe-4S] (0, 8, 60 nM), [2Fe—2S] (64 nM), or apo NsrR (64 nM); only [4Fe-4S] NsrR bound to the DNA [11]. B) LC-MS peaks following reaction of [4Fe-4S] NsrR with NO, corresponding to $[Fe_2(NO)_4]$ and $[Fe_2(NO)_4(S)]$, +232 and + 264 Da, respectively (black line). ^{15}NO (blue line) and ^{57}Fe isotope (red line) shifts unambiguously identify NO containing species [71]. C) Native MS reveals mono- and dinitrosyl complexes of [4Fe-4S] NsrR as the first intermediates of cluster nitrosylation. Native MS data before and after the addition of 11 NO per [4Fe—4S] cluster, showing formation of D) DNIC-, RRE- and E) RBS-like species (as indicated). F) Mechanistic scheme for the nitrosylation of [4Fe-4S] NsrR [68]. (For interpretation of the references to colour in this figure legend, the reader is referred to the web version of this article.)

negative proteobacteria, with members of the Enterobacteriaceae genera of gamma-proteobacteria particularly represented. NsrR also occurs in gram-positive bacteria of the actinobacteria (primarily Streptomycetale and Corynebacteriale) and Firmicutes (mainly Bacilli) genera. Thus, NsrR appears to be advantageous to a wide range of bacteria occupying different niches, suggesting nitrosative stress is a common feature of microbial life [111]. Like RsrR, NsrR also belongs to the Rrf2 transcriptional regulator super family and, where studied, regulates a suite of genes primarily involved in NO detoxification [11,112–114]. This most commonly involves regulation of the *hmp* gene, which encodes a flavohemoglobin that converts NO to NO_3^- under (micro)aerobic conditions [115]. In *Streptomyces coelicolor* (Sc), HmpA1 and NsrR function together to maintain NO homeostasis and attenuate downstream responses (e.g antibiotic production) to this important signalling molecule [116–118].

3.2.1. A cautionary tale about the determination of cluster type

Although initially thought to bind a [2Fe—2S] cluster, subsequent purifications of ScNsrR under strict anaerobic conditions resulted in protein containing a [4Fe—4S] cluster that was strikingly unreactive towards O_2 [119,120]. Commonly used 'protective' low molecular weight thiols (e.g. dithiothreitol (DTT) and beta-mercaptoethanol (BME) were found to bind to the [4Fe—4S] cluster of NsrR, as previously observed for *Bacillus subitilis* NsrR, significantly affecting the CD spectrum of the [4Fe—4S] cluster [11,121]. Subsequent exposure to O_2 resulted in absorption and CD spectra resembling those initially reported for [2Fe—2S] ScNsrR. Through a combination of native MS, resonance Raman and Mössbauer spectroscopies, it was possible to obtain definitive proof for the existence of the [4Fe—4S] cluster in anaerobic NsrR samples (Fig. 5A, black line) [11]. This was confirmed by the crystal structure, which revealed that the cluster is coordinated at the interface of the subunits of the dimer by three Cys residues (generally conserved in Fe—S cluster-binding Rrf2 regulators) from one monomer and an Asp residue from the other (see [4Fe—4S] in Fig. 1) [122]. Native MS was further employed to follow the reaction of [4Fe-4S] NsrR with DTT in the presence of O_2, directly demonstrating conversion to [2Fe-2S] NsrR (Fig. 5A). Subsequent reanalysis of DNA binding showed that [4Fe—4S] NsrR recognised all regulated protomers (*nsrR, hmpA1, hmpA2*), but [2Fe—2S] and apo NsrR did not (Fig. 5A, inset) [11].

3.2.2. Spectroscopic approaches to studies of protein-bound iron-nitrosyls

EPR spectroscopy has been typically used to study the effects of NO on Fe—S clusters. These studies often pointed to dinitrosyl complexes (DNIC) species as the principal products of nitrosylation [123,124]. However, quantification of EPR signals showed that in many cases the DNIC signal accounted for only a small portion of the iron initially present in the Fe—S clusters [125]. Other forms of spectroscopy, including optical (absorbance, CD, etc.), X-ray absorption, Mössbauer, resonance Raman, infra-red (IR) and nuclear vibration resonance (NRVS) have all been used to investigate the nitrosylation process. These studies have provided a useful insight into, principally, the end products of the nitrosylation reaction, indicating that iron-nitrosyl species similar to the well characterised small molecule DNIC, RRE and RBS complexes are formed [126,127].

Studies of a site-differentiated model complex using IR, EPR, NMR, X-ray crystallography and mass spectrometry [128] provided valuable insights into the nitrosylation of [4Fe-4S] model clusters. Reaction proceeded via the formation of a novel tetranitrosyl [4Fe—4S] cluster, $[Fe_4S_4(NO)_4]^-$ (S = ½), prior to the formation of RBS species, $[Fe_4S_3(NO)_7]$. The MS data indicated the formation of a diverse range of iron nitrosyls, principally $[Fe_4S_4(NO)_{1-4}]^-$ and $[Fe_4S_3(NO)_{1-7}]^-$ [128]. Determination of the mechanism of the reaction of NO with [4Fe-4S] NsrR presented a significant challenge because of the rapid rate of reaction and difficulty in distinguishing the nature of the iron-nitrosyl intermediates and products formed [129].

NRVS is not restricted by the selection rules that dominate IR and Raman spectroscopy, and as a result can reveal all vibrational modes of ^{57}Fe nuclei and associated atoms [127,130]. In the case of ^{57}Fe-enriched NsrR, a combination of Mössbauer and NRVS was used along with $^{14/15}$NO and $^{32/34}$S (cluster sulfide) isotope substitutions, revealing that nitrosylation resulted in the production of species related to RBS and RRE, together with small amounts of DNIC. The RBS species was somewhat unusual because no ^{32}S/^{34}S shifts were observed in the NVRS spectra. Subsequent DFT simulations of the NRVS data indicated the existence of a novel RBS species in which one or more of the ^{34}S sulfide ions had been substituted by a naturally abundant ^{32}S protein thiolate, e.g. Cys, to give an RBS-like species, tentatively termed a Roussins' black ester. DTF calculations also provided evidence for cysteine persulfide-ligated forms of RRE and RBS-like species [131].

3.2.3. Application of MS to studies of protein-bound iron-nitrosyls

Clear evidence for RRE and persulfide RRE species bound to NsrR was obtained by LC-MS. Why such species were able to survive under denaturing conditions of LC-MS is not clear but may indicate a relative structural robustness of RRE compared to Fe—S clusters (Fig. 5B) [71,124]. Furthermore, it is noteworthy that reaction of multiple NO molecules to Fe—S clusters typically results in coordination and electron transfer, leading to the oxidation of cluster sulfide to sulfane (S^0) [125], and the consequent observation of persulfide-coordinated RBS-like species.

The reaction of NsrR with NO is an extremely rapid, multiphasic, non-concerted process involving multiple NO molecules per cluster, prior to the formation of stable RRE, RBS-like and DNIC species [68,71,131]. For thermodynamic NO titration experiments, the source of NO was dipropylenetriamine (DPTA) NONOate, which slowly liberates 2 molecules of NO via a first order process [132]. Under defined conditions (of pH and temperature) NO availability is rate-limiting, permitting an in situ titration of [4Fe-4S] NsrR samples with NO, monitored by native MS [68] (Fig. 5C). As noted above, the monomerization of dimeric NsrR during ionisation and ^{57}Fe, ^{34}S, ^{34}S/^{57}Fe isotope substitution was used to simplify data interpretation.

Monomeric [4Fe-4S] NsrR (at 17,824 Da) gradually decayed as the NO concentration increased, and was accompanied by an increase in intensity at 17,854 Da, a mass increase of +30 Da, consistent with the coordination of a single NO (+30 Da) molecule by the [4Fe—4S] cluster [68] (Fig. 5C). Independent evidence for a stable model [4Fe—4S](NO) species was recently reported [133]. A second species very likely corresponding to the coordination of two NO molecules (+60 Da) was also observed to increase in intensity [68]. Species corresponding to [4Fe-4S] $(NO)_{1-2}$ were also observed in biomimetic studies [128], but it was unclear whether these were stable species or the result of ionisation-induced damage to the tetranitrosyl species. ^{34}S and ^{57}Fe isotope substitution data supported the assignment of the +30 Da peak as [4Fe-4S](NO) and not a species with an additional sulfur. Overlapping species prevented an unambiguous assignment of the +60 Da adduct as [4Fe-4S]$(NO)_2$ [68].

At higher [NO]:[4Fe—4S] ratios (≥ 4), NsrR-bound iron-nitrosyls corresponding to DNIC, RRE and RBS-like species were detected. Though some DNIC (17,588 Da, $[Fe(NO)_2]$) formation was observed immediately upon addition of NO, DNICs, including persulfide-coordinated RRE species (17,736 Da, $[Fe_2(NO)_4(S^0)]$), were formed at [NO]:[4Fe—4S] ratios ≥6, in line with earlier LC-MS observations (Fig. 5D) [68,71]. A family of RBS-like species with the general formula $[Fe_4(S)_3(NO)_x]$, where x = 3–6 (Fig. 5E), were also detected, consistent with previous NRVS and MS measurements [68,128,131]. It was noted that, while RBS itself, $[Fe_4(S)_3(NO)_7]$, was not formed, a species, $[Fe_4(S)_2(NO)_7$, a possible intermediate in the conversion of RRE to RBS, was detected [68,134]. All RRE and RBS-like species detected by native MS experiments increased markedly above [NO]:[4Fe—4S] ≥ 6 and exhibited a similar intensity profile, suggesting possible RRE to RBS interconversion, or breakdown of higher mass nitrosyl species [68,134,135].

Thus, native MS data in combination with structural and biophysical data for NsrR have provided a detailed picture of Fe—S cluster nitrosylation (Fig. 5F) [11,68,71,122,129,136]. Further investigations are underway to understand better which of these iron-nitrosyl intermediates are physiologically important in the reaction of NO directly with NsrR-DNA complexes.

3.3. Iron sensing by Fe—S proteins: RirA, a global iron regulator of rhizobia

The global iron regulator RirA, found primarily in alpha-proteobacteria, is also a member of the Rrf2 super family. It performs a role analogous to *E. coli* IscR in regulating Fe—S cluster assembly, in addition to iron acquisition [25,137,138]. Based on homology with IscR, and later NsrR, it was hypothesized that RirA may utilise an Fe—S cluster, and anaerobic purification of RirA following heterologous expression in *E. coli* resulted in broad absorbance across the near UV and visible regions indicative of a mix of [2Fe-2S] and [4Fe-4S] clusters, as previously observed for NsrR [11,58,119]. Post-purification cluster reconstitution resulted in an absorbance spectrum indicative of a [4Fe—4S] cluster [58].

The [4Fe—4S] cluster ligated by RirA was found to be particularly prone to losing iron, especially during gel filtration (Fig. 6A). In combination with EPR, gel filtration was found to give rise to transiently stable $[3Fe—4S]^{1+}$ cluster, suggesting an equilibrium between $[4Fe-4S]^{2+}$ and $[3Fe-4S]^{1+}$ forms, prior to the appearance of [2Fe-2S] RirA species [58]. The [4Fe—4S] form of RirA (and possibly [3Fe-4S] RirA [139]) binds tightly to regulated DNA sequences, consistent with it functioning to repress expression. Under low iron conditions, the [4Fe—4S] cluster of RirA degrades to a [2Fe—2S] form (Fig. 6B), which

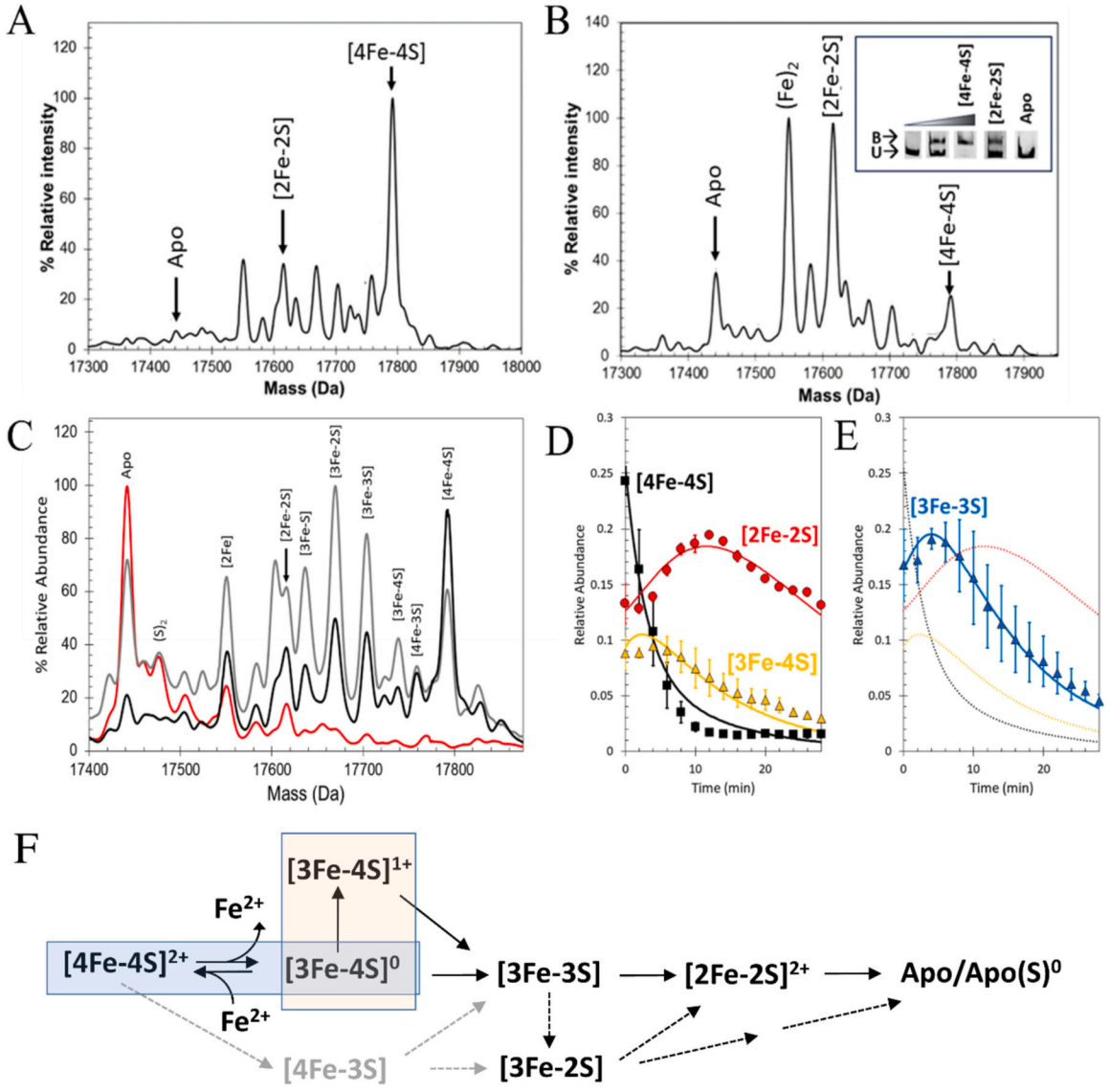

Fig. 6. Mass spectrometric characterisation of [4Fe-4S] RirA reveals mechanism of iron sensing. Native MS spectra of [4Fe-4S] RirA A) before and B) after low iron mediated cluster conversion. Inset in B) shows the effect on DNA binding. DNA containing the *fhuA* promoter sequence was treated with [4Fe-4S] (0, 209, 418 nM), [2Fe—2S] (417 nM), and Apo-RirA (422 nM). Both [4Fe-4S] and [2Fe-2S] RirA bind DNA but have differing affinities [58]. C) Time resolved native MS spectra, recorded during low iron mediated cluster conversion recorded at 0 (black line), 4 (grey line) and 30 min (red line) following exposure to low iron conditions; mechanistically important species are labelled. D) Relative abundances of [4Fe-4S] (black squares), [3Fe—4S] (yellow triangles), [2Fe—2S] (red circles) and E) [3Fe—3S] (blue triangles) as a function of time after exposure. Solid lines in D and E represent fits of the experimental data using the reaction scheme depicted in F). The blue and pink boxes indicate the iron and O_2 sensing steps, respectively. Dashed arrows indicate minor pathways; grey dashed arrows indicate a likely artefact of ionisation. Dashed lines in E show fits of [4Fe-4S], [3Fe—4S] and [2Fe-2S] data to enable comparison [70]. (For interpretation of the references to colour in this figure legend, the reader is referred to the web version of this article.)

binds much less tightly to DNA. The [2Fe—2S] cluster eventually degrades to apo RirA, which has little affinity for DNA and thus no longer represses expression (Fig. 6B, inset) [58].

3.3.1. Elucidation of the RirA iron-sensing mechanism using native MS

The native MS spectrum of RirA contained a peak at 35,585 Da corresponding to the [4Fe—4S] RirA homodimer, as well as a secondary, lower mass peak due to a dimer containing one [3Fe—4S] and one [4Fe—4S] cluster. The monomeric region (arising from partial dissociation during ionisation [78]) contained an intense peak at 17,792 Da due to [4Fe-4S] RirA but several well-resolved peaks were also observed due to RirA containing [4Fe—3S], [3Fe—4S], [3Fe—3S], [3Fe—2S] and [2Fe-2S] clusters. The detection of a [3Fe—4S] form of RirA following desalting (in preparation for native MS) was consistent with the above gel filtration and EPR observations (Fig. 6A) [58,70].

Native MS analysis of [4Fe-4S] RirA under anaerobic, low-iron conditions indicated that, after 30 min, [4Fe—4S] RirA was replaced by [2Fe] and [2Fe-2S] RirA (at 17,550 and 17,615 Da, respectively, Fig. 6B). RirA homodimers containing mixtures of [4Fe-4S], [3Fe—4S], [3Fe—3S] and [2Fe–3S] were observed, consistent with conversion of [4Fe–4S] into [2Fe–2S] clusters over this time period. Native MS was then used in real time to monitor cluster degradation following exposure to low iron (through addition of an iron chelator). [4Fe—4S] RirA gradually decayed away and new peaks due to formation of protein-bound [4Fe-3S], [3Fe—4S], [3Fe—3S], [3Fe—S], [2Fe—2S] and [2Fe-2S] (17,856–17,762 Da) cluster breakdown species were formed. These subsequently decayed to yield apo RirA (with sulfur adducts) (Fig. 6C). Using the program Dynafit, MS and EPR data were fitted in order to generate a mechanistic model, see Fig. 6E [70].

The same cluster intermediates were observed under low-iron conditions in the presence of O_2, but several steps of the reaction downstream of the $[3Fe—4S]^{0/1+}$ intermediate occurred at an enhanced rate. Overall, observations indicated that, irrespective of the presence of O_2, the initial step corresponds to the reversible loss of an Fe^{2+} ion from the [4Fe—4S] cluster to form the $[3Fe—4S]^0$ cluster, reminiscent of aconitase in terms of cluster stability [20]. This first intermediate is susceptible to oxidation by O_2 [58,70]. Hence, Eq. (6) represents the iron-sensing reaction.

$$[4Fe-4S]^{2+} \Leftrightarrow [3Fe-4S]^{0} + Fe^{2+} \quad (6)$$

Thus, when iron is limiting, the $[3Fe—4S]^0$ cluster would be expected to accumulate as the reverse association of Fe^{2+} with the [3Fe—4S] cluster would be unfavourable due to low Fe^{2+} availability. The relatively unstable $[3Fe—4S]^0$ intermediate undergoes a rearrangement to generate a [2Fe—2S] cluster, leading to the de-repression of RirA-regulated genes. If this is correct, then the affinity of Fe^{2+} for the $[3Fe—4S]^0$ cluster should be in the physiological range, and this was found to be the case, with a K_d of ~3 μM. The susceptibility of $[3Fe\text{-}4S]^0$ to O_2-mediated oxidation (to $[3Fe\text{-}4S]^{1+}$) can be viewed as the key step in the proposed mechanism of O_2 sensing (Fig. 6F), because cluster degradation occurs more rapidly when O_2 is present [58,70,73].

3.3.2. The fourth ligand to the RirA [4Fe—4S] cluster

A key question about RirA is why is the RirA [4Fe—4S] cluster so susceptible to loss of an iron and subsequent degradation? Phylogenetic analysis of the Rrf2 family revealed a close relationship between the RirA and NsrR clades [140]. As discussed in Section 3.2, the [4Fe—4S] cluster of NsrR is coordinated by three Cys residues and one Asp (at position 8) from the other subunit of the dimer [122]. Homology modelling of RirA, based on the NsrR structure [73], highlighted that Asn8, the RirA residue equivalent to Asp8 of NsrR, is in the correct location to potentially coordinate the cluster, but is predicted to be pointing away from the cluster (Fig. 7A). Importantly, Asn is not a recognised ligand of Fe—S clusters, leading to the proposal that RirA may have only three amino acid residue ligands (the three conserved Cys residues) [70,73]. Substitution of Asn8 with Asp resulted in a variant protein with a visible CD spectrum very similar to that of NsrR (Fig. 7B), suggesting that the N8D variant of RirA has cluster coordination very similar to that of NsrR [73]. Furthermore, the cluster of the variant was much more stable than that of the wild-type protein (Fig. 7C), and was no longer sensitive to iron chelators. The variant protein retained high affinity DNA-binding activity and in vivo experiments with a *Rhizobium leguminosarum rirA*$^-$ mutant strain complemented with a gene encoding N8D RirA demonstrated that it functioned as a repressor of iron uptake but had lost the ability to sense iron levels [73]. Thus, collective observations of the wild-type and N8D variant proteins support the suggestion that the site-differentiated iron of the cluster (i.e. the one not coordinated by a Cys thiolate) is labile and may not be coordinated by the protein at all. Efforts towards a high-resolution structure of the protein are ongoing, while other spectroscopic methods, such as resonance Raman, could be used in the future to probe the nature of the fourth ligand in the absence of structural data.

4. Wbl-like (Wbl) proteins: non-canonical Fe—S cluster regulators

The WhiB-like (Wbl) family of proteins are found exclusively in Actinobacteria and associated viruses [141–143]. Wbl proteins are known to play key roles in the virulence and antibiotic resistance of pathogenic Mycobacteria and Corynebacteria species (e.g,

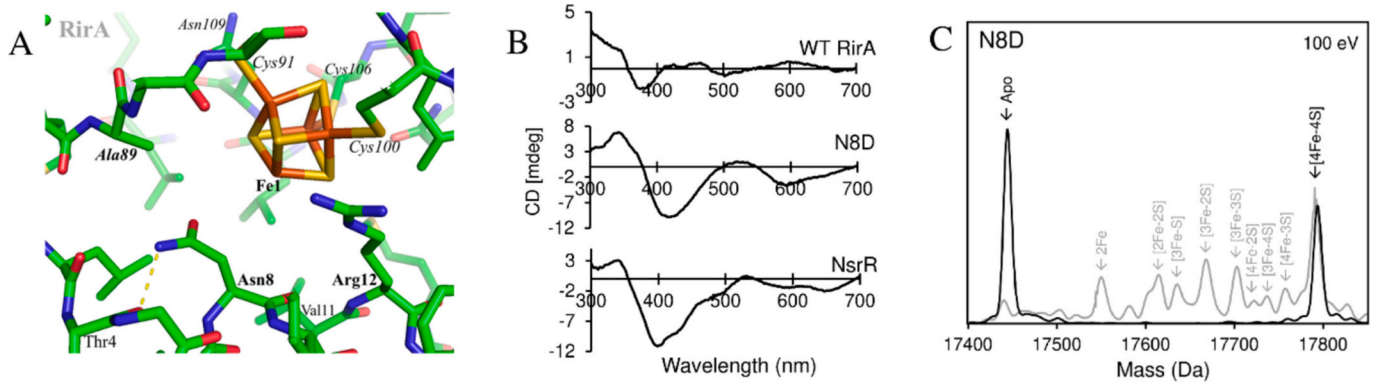

Fig. 7. The N8D variant of RirA contains a stable, NsrR-like [4Fe—4S] cluster. A) Structural model of [4Fe-4S] RirA based on [4Fe-4S] NsrR. The side chain of Asn8 is predicted to face away from the cluster to avoid clashes with either Arg12 or the cluster. The illustrated conformation is stabilised by a H-bond to the carbonyl of Thr4. B) CD spectra of reconstituted wild-type (WT) RirA, and the as-isolated variant N8D. The spectrum of *S. coelicolor* NsrR is also shown for comparison. C) Mass spectrum of the monomeric region of N8D RirA (with 100 eV in source collision induced dissociation applied) showing apo and [4Fe-4S] N8D RirA, with no observed cluster degradation species. The equivalent spectrum of wild-type RirA is shown in grey for comparison.

M. tuberculosis, *C. diphtheriae*), but are equally important in the physiology of non-pathogenic actinobacteria species [141,144]. Where studied, Wbl proteins have been shown to bind an O_2 and/or NO sensitive [4Fe—4S] cluster [142,145–154] and can be separated into five distinct classes (I – V), with WhiB1, WhiB2, WhiB3, WhiB4 and WhiB7 being the archetypal member of each class, respectively. *M. tuberculosis* WhiB1 (MtWhiB1), *S. coelicolor* WhiB (class II, ScWhiB), and WhiD (class III) from *S. coelicolor* (ScWhiD) and *S. venezuelae* (SvWhiD) display CD properties very similar to each other (Fig. 8A), consistent with the high degree of sequence conservation within this protein family [141]. Although broadly annotated as DNA-binding transcriptional regulators, only WhiB7-like class V proteins contain a recognisable AT-hook DNA-binding motif [141,148,155].

4.1. Role of Wbl proteins in regulating transcription

MtWhiB1 is essential for cell viability in vivo. In vitro, [4Fe—4S] WhiB1 does not recognise the *whiB1* promotor (Fig. 8B, inset), but [4Fe—4S] WhiB1 readily binds to the principal housekeeping sigma factor (σ^A) in a cluster-dependent manner (Fig. 8B) [147,150,154]. In contrast, apo WhiB1 binds to the *whiB1* promotor (Fig. 8B, inset), among others, inhibiting transcription, even in the presence of the cognate transcriptional activator [150,156]. *M. tuberculosis* WhiB3 (termed WhiD in *Streptomyces* sp.) contributes to the survival and pathogenesis of *M. tuberculosis* but is dispensable for growth [149,157]. Like most Wbl proteins, [4Fe—4S] WhiB3 also binds to the principal sigma factor (σ^A), regulating the expression of genes involved in the biosynthesis of lipids (e.g. tri-acylglycerol) and polyketides in response to activated macrophages, leading to the suggestion that WhiB3 acts as a sensor of reactive O_2 or NO species [149,153,157]. More recent structural studies have revealed that Wbl:σ^A complexes share a common molecular interface and possess a newly defined Arg-rich C-terminal DNA-binding motif, while cyo-EM structures show how Wbl-proteins interact with DNA and the transcription machinery to elicit transcription [148,153,154,158].

4.2. Native MS studies of Wbl:SigA complexes and the effects of nitrosylation

The interaction of Wbl proteins with the C-terminal domain of σ^A (σ^A-CTD) has been studied by native MS. Both MtWhiB1 and SvWhiD demonstrated [4Fe-4S] cluster-dependent 1:1 complex formation with σ^A–CTD (Fig. 8C), consistent with structural observations (Fig. 8C, inset) [152–154]. These complexes showed little (WhiD) or no (WhiB1) sensitivity to O_2, but reacted rapidly with NO, resulting in loss of the Wbl:σ^A-CTD complex. These observations are consistent with a role for these proteins in NO sensing (Fig. 8D) [125,147,151].

Native MS showed that reaction of uncomplexed [4Fe-4S] WhiD with NO led to loss of the [4Fe—4S] cluster, as observed for NsrR. However, the two proteins exhibited very different decay behaviour. For WhiD, the [4Fe—4S] species was gradually lost through the titration, and was completely absent only at [NO]:[4Fe—4S] $\geq$ 10, consistent with earlier spectroscopic studies. This is indicative of a reaction mechanism where NO-reacted clusters are more susceptible to further reaction with NO than unreacted clusters. Peaks at +30 Da, +60 Da relative to [4Fe-4S] WhiD, were detected over a broad ratio of NO:[4Fe-4S] cluster, up to the point where the [4Fe—4S] WhiD peak was lost (Fig. 8E). ($^{57}Fe/^{34}S$ isotope shift analyses were consistent with formation of [4Fe–4S](NO) and [4Fe–4S](NO)$_2$ intermediates [68]. At higher levels of NO, an additional peak at +120 Da, possibly due to a putative tetra-nitrosylated cluster, [4Fe—4S](NO)$_4$, was also observed (Fig. 8E). This appeared to transition into a RBS-like species, reminiscent of observations made for small molecule clusters model compounds [68,128].

5. Fe—S cluster biogenesis: insights from mass spectrometry

Although iron-sulfur clusters can spontaneously assemble, living organisms require multi-protein machineries that synthesise Fe—S clusters de novo and deliver them to client proteins [159,160]. *E. coli* has two Fe—S biogenesis machineries, the Isc (*iscRSUA-hscAB-fdx-iscX*) and Suf (*SufABCDSE*) systems. These are respectively employed under conditions of normal growth and oxidative stress/iron limitation [161,162]. Minimalist Fe—S assembly systems (MIS) are also found in some organisms, and likely evolved before their more complex multi-protein counterparts. MIS systems typically comprise of a cysteine desulfurase and a scaffold protein on which the cluster is built, with iron acquisition being an inherent property of the desulfurase-scaffold complex (e.g. IscSU) [163,164]. For example, the human pathogen *Helicobacter pylori* has such a minimalist Fe—S assembly system (NifSU), which is essential for viability and is functionally exchangeable with the *E. coli* IscSU proteins [165].

The desulfurase (IscS) and scaffold (IscU) of the Isc system have been extensively studied. Crystal structures of various bacterial IscS and IscU proteins, alone and or in complex with each other (PDB: 3LVM, 3LVL, 3LVJ, 4EB7. 4 EB5, 2L4X) have provided key insights into the mechanism of intramolecular sulfur transfer and associated protein-protein interactions that underpin the Fe—S assembly process [166–169]. Briefly, IscS is a cysteine desulfurase, which employs a pyridoxal phosphate (PLP) cofactor to catalyse the conversion of L-cysteine to L-alanine, releasing sulfane (S^0). The S^0 is stored as a persulfide on a conserved cysteine residue of IscS. In concert with the scaffold protein (IscU), a [2Fe—2S] cluster is initially assembled on IscU, prior to the cluster being delivered to apo protein clients [161]. IscS also provides S^0 to other cellular processes requiring sulfur (e.g. TusA), and its activity is subject to allosteric regulation by accessory proteins, e.g. IscX and CyaY [169,170]. The binding site of these accessory proteins (e.g. IscX, CyaY, TusA) overlap with each other and another important protein, Fdx, which provides reducing equivalents needed to reduce S^0 to sulfide S^{2-} (Fig. 9A) [171,172].

5.1. Native MS studies of ISC Fe—S cluster biogenesis

The interaction of IscS with IscU and/or accessory proteins (IscA, HscAB, Fdx, IscX, CyaY) has been studied by various techniques (principally NMR and crystallography). While many of the stable complexes have been elucidated, higher order, possibly transient complexes involving IscSU and one or more accessory proteins may exist [173]. Native MS has been employed to study such complexes involving IscS, including the sequential formation of $(IscS)_2(IscU)$ and $(IscS)_2(IscU)_2$ complexes at increasing concentrations of IscU relative to IscS [174,175], and complex formation between IscS and two other proteins: IscU and IscX (e.g. Fig. 9B) [171] or IscU and CyaY [173]. These studies confirmed that IscU does not compete with CyaY or IscX for IscS [171,173]. Native MS also confirmed the preference of $(IscS)_2$ for apo CyaY over Fe-CyaY, consistent with solution studies. Taken together, the native MS observations indicate that dimeric IscS harbours two independent binding sites for IscU (K_d of ~3 μM), together with two further binding sites for accessory proteins (e.g CyaY, IscX), consistent with previous observations (Fig. 9B) [168,169,171,174,175].

Native MS has also been used to probe mechanistic aspects of Fe—S assembly on the IscSU complex. Major challenges exist for the application of this technique in this context, most notably the efficient ionisation of large IscS-IscU complexes (~105 to 120 kDa) and achieving sufficient resolution to enable binding of single atoms (e.g ^{32}S, ^{34}S, ^{56}Fe, ^{57}Fe) to these large complexes to be detected. For this reason, studies have thus far been confined to the detection of Fe—S species associated with IscU (Fig. 9C) [174,175].

Native MS of as-isolated IscU demonstrated one Zn^{2+} ion bound per IscU monomer (Zn-IscU), consistent with previous observations (Fig. 9C, black line). Various biophysical approaches have shown IscU to be a dynamic protein that can exist in different conformational states in vitro; principally the structured (S) and disordered (D) states [176,177]. The S-state of IscU is stabilised by Zn^{2+} and this ion is resistant to

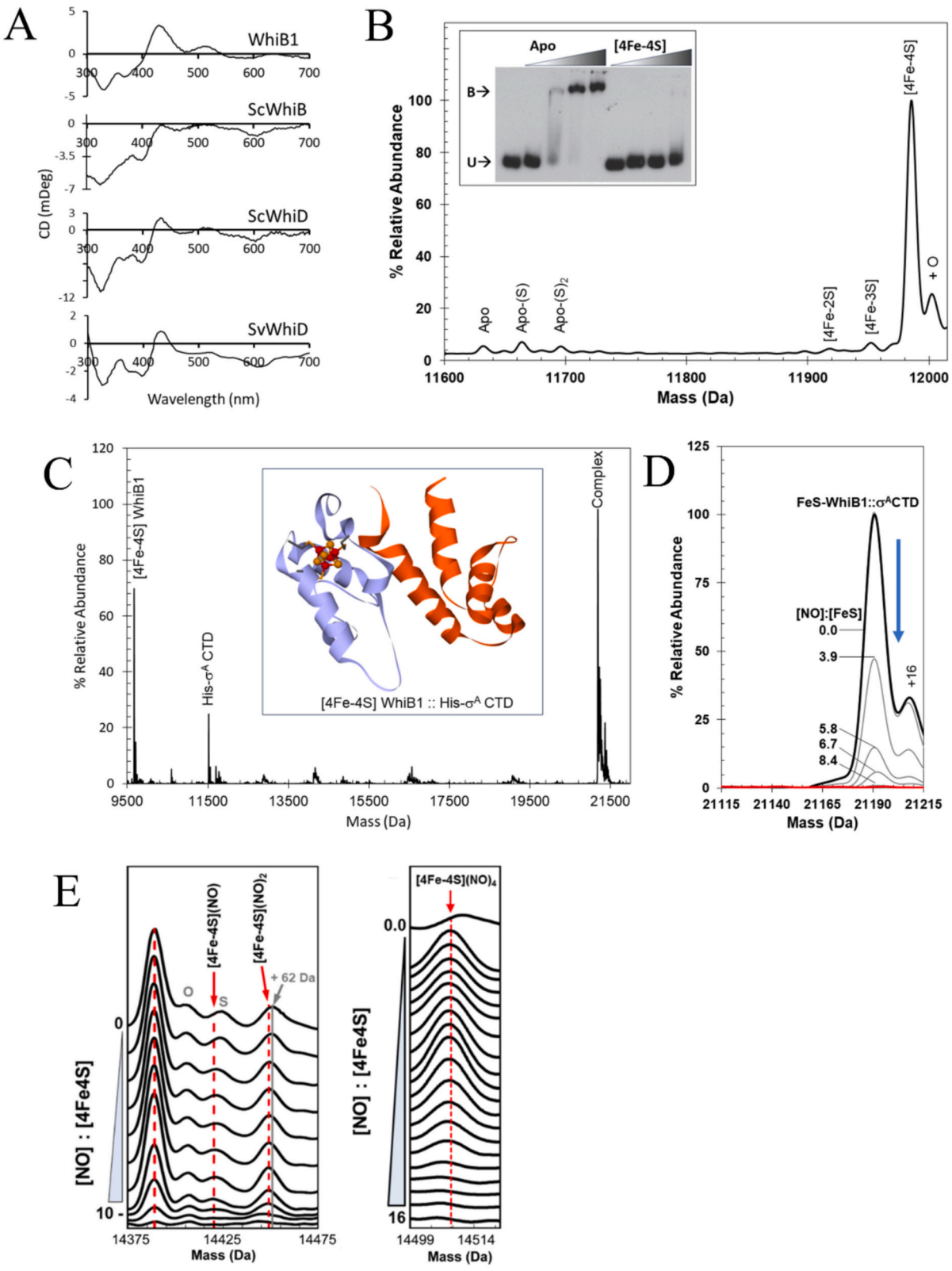

Fig. 8. Spectroscopic and mass spectrometric characterisation of Wbl proteins and complexes. A) CD spectra of WhiB1, ScWhiB (unpublished data), ScWhiD and SvWhiD [145,150,151]. B) Native MS spectrum of His-tagged [4Fe-4S] WhiB1; inset shows the effect on DNA binding [147,150]. DNA containing the *whiB1* promoter sequence was treated with increasing amounts of apo and [4Fe-4S] WhiB1; only apo WhiB1 bound to the DNA [150]. C) Native MS of [4Fe-4S] WhiB:His-σ^A-CTD complex, a partial disassembly into constituent parts [147]; inset shows crystal structure of [4Fe-4S] WhiB:His-σ^A-CTD complex (PDB: 6ONO) [154]. D) Native MS shows [4Fe-4S] WhiB:His-σ^A-CTD complex disassembly in response to NO [147]. E) Detection of mono-, di- and tetra-nitrosyl forms of uncomplexed [4Fe-4S] ScWhiD [68].

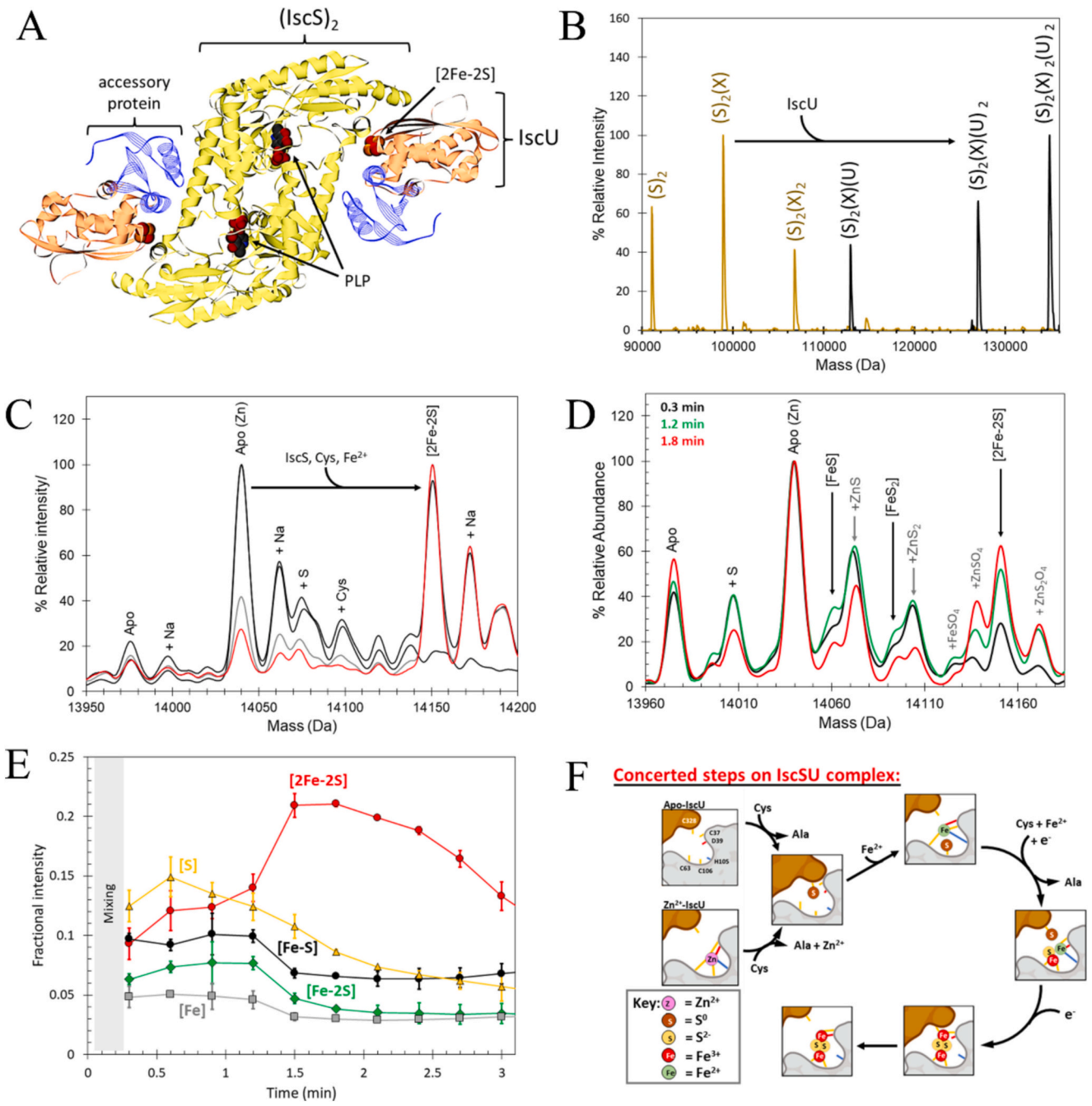

Fig. 9. Mass spectrometric characterisation of Isc proteins and complexes. A) Ribbon diagram representing $(IscS)_2(IscU)_2$ in complex with accessory proteins (e.g. TusA, IscX, CyaY or Fdx,); PLP and [2Fe-2S] cofactors indicated in space filling mode (PDB: 4EB5, 3LVJ) [168,169]. B) Native MS data showing the binding of (IscU) to pre-formed $(IscS)_2(IscX)_{1-2}$ complexes (yellow line), resulting in higher order complexes (black line), including $(IscS)_2(IscX)_2(IscU)_2$. (unpublished data). C) Time-resolved native MS of the biomimetic reconstitution reaction in the un-complexed IscU region. The starting and final spectra are black (0 min) and red (25 min), respectively, intervening spectra are grey (10 min); major species as indicated [174]. D) Non-IscS-mediated reconstitution reaction reveals assembly intermediates of [2Fe-2S] IscU. Spectra were recorded at 0.3, 1.2, and 1.8 min from the start of the reaction, major species are as indicated [174]. E) Kinetic behaviour of intermediate species Note that the gradual loss of [2Fe-2S] IscU, as noted elsewhere, is consistent with the increased lability of the [2Fe—2S] cluster in native MS buffers [174,175,179]. F) Scheme describing the concerted mechanism of [2Fe-2S] assembly on IscU in complex with IscS. Exact details of S- and Fe- binding/transfer are based on literature [174,175,179,184–186]. (For interpretation of the references to colour in this figure legend, the reader is referred to the web version of this article.)

displacement by Fe^{2+} ions or physiologically relevant low molecular weight thiols (e.g. L-Cys, GSH), resulting in a significantly lower rate of [2Fe-2S] cluster formation on IscU [174,175,178]. Importantly, the presence of Zn^{2+} ions bound to IscU does not adversely affect its association with IscS, and both $(IscU)_2(IscS)_2$ and $(IscU)(IscS)_2$ complexes were readily observed by native MS [174,175].

Treatment of IscSU complexes with L-cysteine promotes the removal of Zn^{2+} ions from Zn-IscU, through the IscS-mediated formation of S^0/S^{2-}[174,175]. This process occurs even in the absence of Fe^{2+} ions, where Fe—S assembly cannot proceed [174]. Thus, transfer of the persulfide formed on IscS-Cys328 to IscU may trigger the displacement of Zn^{2+}, perhaps by altering the binding environment to reduce the affinity of the site for Zn^{2+} [174,175,179]. We note that recent ion mobility native MS studies indicated that, upon binding to IscS, the S-state of Zn-

IscU shifts towards the D-state, adopting an intermediary conformation that facilitates Zn^{2+} displacement [179]. We also note that for the IscU-like protein SufU from *M. tuberculosis*, a bound Zn^{2+} ion plays an important role in the S^0/S^{2-} transfer reaction between the cysteine desulfurase (SufS) and SufU [180]. Thus, Fe^{2+} binding does not appear to be a pre-requisite for S^0 transfer [174].

Time-resolved native MS has also been used to probe the formation of intermediates species. Lin et al [175] studied the formation of intermediates on un-complexed IscU (produced through in source disassociation of the $(IscU)_2(IscS)_2$ complex) during Fe—S assembly. Low quantities of [Fe], [Fe_2], [Fe—S], [S] and [S_2] forms of IscU were found to rapidly form, and then declined as the [2Fe—2S] IscU product was formed [175]. Our own, independent reconstitutions, employing catalytic quantities of IscS, were also monitored by time-resolved native MS. The intensity of un-complexed Zn-IscU (or apo IscU) decreased, with a concomitant increase in the amount of [2Fe-2S] IscU, but significant Fe—S intermediates were not observed on IscU (Fig. 9C) [174], suggesting that assembly occurs in a concerted manner. However, sub-optimal S^0 transfer to IscU via a low molecular weight IscS mimic (see [174] for details) did reveal peaks consistent with the presence of IscU-bound [S], [Fe—S], [Fe—2S] and [2Fe-2S] (Fig. 9D). The kinetic data indicated that [S] species form first, followed by [Fe-S] and [Fe-2S], and then, finally, the [2Fe—2S] cluster (Fig. 9E), and were in agreement with observations that S transfer could occur in the absence of iron [174].

Taken together, these native MS studies indicate that the FeS assembly carried out by the IscSU complex is a largely concerted process, with respect to IscU, such that partly assembled, intermediary Fe—S clusters do not readily accumulate and are thus hard to detect (on un-complexed IscU). The studies also indicate that order of Fe^{2+} binding or sulfur transfer does not appear to matter in vitro (Fig. 9F) [174,179]. Instead, they indicate that Zn^{2+} ions provide stability, potentially protecting un-complexed IscU until a binding site becomes available on IscS [174,175,179]. Thus, cluster assembly on IscU is controlled by sulfur availability, with sulfur transfer leading to Zn^{2+} displacement and is thus a key step [174]. This proposal is also consistent with role of CyaY in the allosteric regulation of IscS desulfurase activity [180].

Comparable protein-protein interactions are similarly important for the human ISC FeS cluster biogenesis system [160]. Here, native MS has been used investigate the post-assembly process of Fe—S cluster trafficking towards client proteins. The data provides evidence for a [2Fe—2S]-cluster-bridged form of homodimeric glutaredoxin 5 (GLRX5), as well as the existence of a GLRX5:BolA-like protein 3 (BOLA3) heterodimer. In the presence of a client protein, a ferredoxin (FDX2), GLRX5 formed a unique hetrodimeric (FDX2:GLRX5:[2Fe—2S]:GSH), that provides important new insight into process of Fe—S trafficking and delivery [181].

5.2. *New approaches to identifying Fe—S proteins involved in assembly, trafficking and delivery*

Strategies to monitor Fe—S cluster assembly, trafficking and delivery in the cytosol are now emerging. Recently, a powerful proteomic LC-MS methodology, known as isotopic tandem orthogonal proteolysis-activity based protein profiling (IsoTOP-ABPP) was reported [72]. Briefly, IscoTOP-ABPP can be used to quantitatively monitor changes in the reactivity of cysteine residues towards a cysteine thiolate-reactive probe (e.g. iodoacetamide-alkyne) within the proteome of an organism [182,183]. Interrogation of the proteome of *E. coli* using this approach resulted in identification of known Fe—S proteins (e.g FNR, BioB, Fdx), known participants in Fe—S assembly, trafficking, and delivery (e.g. IscU, SufA, ErpA), in addition to previously uncharacterised Fe—S proteins (e.g. TrhP) [72]. This technique has great potential and may become useful tool in the study of eukaryotic Fe—S assembly, trafficking, and delivery.

6. Outlook

Applications of native MS to metalloprotein systems, and particularly Fe—S cluster proteins, have expanded greatly in recent years, partly driven by the increasing availability of relatively low-cost high-resolution instrumentation, and through the development of methodologies that permit routine handling of difficult to work with (e.g. O_2-sensitive) proteins to be studied. Ground-breaking time-dependent native MS measurements have provided unprecedented resolution of complex reaction mechanisms in which the Fe—S cluster is the site of physiologically relevant chemical changes. The power of the technique lies in its capacity to detect and identify all protein-associated Fe—S species simultaneously, and track their relative concentrations over time, using protein samples of micromolar concentration. It is most effective when used in combination with spectroscopic and structural methods, which can provide chemical and oxidation state information that provides key context for the mass information provided by native MS.

Current limitations relate to difficulties in optimising conditions and instrument parameters for efficient ionisation. For example, selection of an appropriate volatile buffer, its concentration, and pH to enable formation of ions whilst retaining tertiary/quaternary structure varies according to the protein sample. This bottleneck means that native MS studies are not routine and require a significant investment of time and, of course, good access to a suitable instrument. A further current limitation relates to limits of resolution at high m/z values. Thus, large proteins or protein complexes that do not readily ionise, or acquire significant charge, may be difficult to detect with sufficient resolution. While this does not significantly affect ability to detect protein complexes (and thus to determine stoichiometry), which involve large changes in mass (i.e. multiple kDa differences between different complexes), it does limit ability to detect relatively small (tens of Da) mass changes that accompany chemical reactions, for example, at the active site of a protein. Ever advancing improvements in methodologies, instrumentation hardware and associated software constantly push back the boundaries of what is possible, opening up larger proteins systems to investigation by native MS. Indeed, we expect to see a significant broadening in application of native MS in the next few years.

Some MS approaches and technologies that we expect to have a significant impact for metalloprotein studies include ion mobility separation. This increasingly useful technique permits ions of identical m/z to be resolved according to their cross-sectional area (shape) [187]. Thus, it is possible to separate different conformations of proteins. This additional means to separate/isolate specific ions also enables low intensity ions, that would otherwise be lost in the baseline of a conventional measurement, to be detected, effectively increasing the sensitivity of native MS measurements. This opens up possibilities to detect very low abundance intermediates of Fe—S cluster reactivity. Another area that we expect to become more important as methodologies are developed and improved is the application of native MS to cells, i.e. without the need for extensive protein purification [188,189]. This presents many challenges in terms of achieving ionisation, but there are already reports of successful measurements from cell lysates or whole cells [190].

In summary, tremendous recent progress has been made in the application of native MS to a range of Fe—S sulfur cluster proteins and to studies of their assembly. Native MS is rapidly becoming an essential tool for mechanistic studies because of its ability to resolve closely related cluster species that cannot be distinguished by other methods.

CRediT authorship contribution statement

Jason C. Crack: Writing – review & editing, Writing – original draft, Conceptualization. **Nick E. Le Brun:** Writing – review & editing, Writing – original draft, Conceptualization.

Consent to participate

This article does not contain any studies with human participants and therefore did not require any consent to participate.

Ethics approval

This article does not contain any studies with human participants or animals performed by any of the authors.

Declaration of competing interest

The authors declare that there are no competing or conflicts of interest.

Acknowledgements

The authors thank Prof Annalisa Pastore and colleagues for supplying IscS and IscX proteins for native MS experiments. The authors acknowledge support from: the UK's Biotechnology and Biological Sciences Research Council (BBSRC) for their work on Fe—S cluster regulators over many years, and UEA for the purchase of an ESI-Q-TOF instrument, and UEA and the British Mass Spectrometry Society for assistance in maintenance of the instrument. This article is based upon work from COST Action FeSImmChemNet, CA21115, supported by COST (European Cooperation in Science and Technology).

Data availability

Data will be made available on request.

References

[1] H. Beinert, J. Meyer, R. Lill, Iron–sulfur proteins, in: W.J. Lennarz, M.D. Lane (Eds.), Encyclopedia of Biological Chemistry, Elsevier, New York, 2004, pp. 482–489.
[2] J.A. Imlay, Iron-Sulphur clusters and the problem with oxygen, Mol. Microbiol. 59 (2006) 1073–1082.
[3] J. Balk, M. Pilon, Ancient and essential: the assembly of iron-sulfur clusters in plants, Trends Plant Sci. 16 (2011) 218–226.
[4] E. Camprubi, S.F. Jordan, R. Vasiliadou, N. Lane, Iron catalysis at the origin of life, IUBMB Life 69 (2017) 373–381.
[5] M.T. Werth, H. Sices, G. Cecchini, I. Schroder, S. Lasage, R.P. Gunsalus, M. K. Johnson, Evidence for non-cysteinyl coordination of the [2Fe-2S] cluster in *Escherichia coli* succinate dehydrogenase, FEBS Lett. 299 (1992) 1–4.
[6] A. Volbeda, M.T.P. Martinez, J.C. Crack, P. Amara, O. Gigarel, J.T. Munnoch, M. I. Hutchings, C. Darnault, N.E. Le Brun, J.C. Fontecilla-Camps, Crystal structure of the transcription regulator RsrR reveals a [2Fe-2S] cluster coordinated by Cys, Glu, and his residues, J. Am. Chem. Soc. 141 (2019) 2367–2375.
[7] A.S. Fleischhacker, A. Stubna, K.L. Hsueh, Y. Guo, S.J. Teter, J.C. Rose, T. C. Brunold, J.L. Markley, E. Munck, P.J. Kiley, Characterization of the [2Fe-2S] cluster of *Escherichia coli* transcription factor IscR, Biochemistry 51 (2012) 4453–4462.
[8] P. Zanello, Structure and electrochemistry of proteins harboring iron-sulfur clusters of different nuclearities, Part I. [4Fe-4S] and [2Fe-2S] iron-sulfur proteins, J. Struct. Biol. 200 (2017) 1–19.
[9] E.F. Pettersen, T.D. Goddard, C.C. Huang, E.C. Meng, G.S. Couch, T.I. Croll, J. H. Morris, T.E. Ferrin, U.C.S.F. ChimeraX, Structure visualization for researchers, educators, and developers, Protein Sci. 30 (2021) 70–82.
[10] C.W. Carter Jr., J. Kraut, S.T. Freer, R.A. Alden, L.C. Sieker, E. Adman, L. H. Jensen, A comparison of Fe_4S_4 clusters in high-potential iron protein and in ferredoxin, Proc. Natl. Acad. Sci. U. S. A. 69 (1972) 3526–3529.
[11] J.C. Crack, J. Munnoch, E.L. Dodd, F. Knowles, M.M. Al Bassam, S. Kamali, A. A. Holland, S.P. Cramer, C.J. Hamilton, M.K. Johnson, A.J. Thomson, M. I. Hutchings, N.E. Le Brun, NsrR from *Streptomyces coelicolor* is a nitric oxide-sensing [4Fe-4S] cluster protein with a specialized regulatory function, J. Biol. Chem. 290 (2015) 12689–12704.
[12] M.K. Johnson, Iron-sulfur proteins: new roles for old clusters, Curr. Opin. Chem. Biol. 2 (1998) 173–181.
[13] J.M. Mouesca, L. Noodleman, D.A. Case, B. Lamotte, Spin-densities and spin coupling in iron-sulfur clusters - a new analysis of hyperfine coupling constants, Inorg. Chem. 34 (1995) 4347–4359.
[14] L. Noodleman, C.Y. Peng, D.A. Case, J.M. Mouesca, Orbital interactions, electron delocalization and spin coupling in iron-sulfur clusters, Coord. Chem. Rev. 144 (1995) 199–244.
[15] T.A. Stich, Characterization of paramagnetic iron-sulfur clusters using electron paramagnetic resonance spectroscopy, Meth. Mol. Biol. 2353 (2021) 259–280.
[16] M.E. Pandelia, N.D. Lanz, S.J. Booker, C. Krebs, Mössbauer spectroscopy of Fe/S proteins, Biochim. Biophys. Acta 2015 (1853) 1395–1405.
[17] B. Zhang, J.C. Crack, S. Subramanian, J. Green, A.J. Thomson, N.E. Le Brun, M. K. Johnson, Reversible cycling between cysteine persulfide-ligated [2Fe-2S] and cysteine-ligated [4Fe-4S] clusters in the FNR regulatory protein, Proc. Natl. Acad. Sci. U. S. A. 109 (2012) 15734–15739.
[18] D. Mitra, V. Pelmenschikov, Y. Guo, D.A. Case, H. Wang, W. Dong, M.L. Tan, T. Ichiye, F.E. Jenney, M.W. Adams, Y. Yoda, J. Zhao, S.P. Cramer, Dynamics of the [4Fe-4S] cluster in *Pyrococcus furiosus* D14C ferredoxin via nuclear resonance vibrational and resonance Raman spectroscopies, force field simulations, and density functional theory calculations, Biochemistry 50 (2011) 5220–5235.
[19] H. Beinert, R.H. Holm, E. Munck, Iron-sulfur clusters: nature's modular, multipurpose structures, Science 277 (1997) 653–659.
[20] H. Beinert, M.C. Kennedy, Aconitase, a two-faced protein: enzyme and iron regulatory factor, FASEB J. 7 (1993) 1442–1449.
[21] G. Layer, D.W. Heinz, D. Jahn, W.D. Schubert, Structure and function of radical SAM enzymes, Curr. Opin. Chem. Biol. 8 (2004) 468–476.
[22] S.J. Booker, R.M. Cicchillo, T.L. Grove, Self-sacrifice in radical S-adenosylmethionine proteins, Curr. Opin. Chem. Biol. 11 (2007) 543–552.
[23] J.C. Crack, J. Green, A.J. Thomson, N.E. Le Brun, Iron-sulfur clusters as biological sensors: the chemistry of reactions with molecular oxygen and nitric oxide, Acc. Chem. Res. 47 (2014) 3196–3205.
[24] J.L. Giel, A.D. Nesbit, E.L. Mettert, A.S. Fleischhacker, B.T. Wanta, P.J. Kiley, Regulation of iron-sulphur cluster homeostasis through transcriptional control of the Isc pathway by [2Fe-2S]-IscR in *Escherichia coli*, Mol. Microbiol. 87 (2013) 478–492.
[25] E.L. Mettert, P.J. Kiley, How is Fe-S cluster formation regulated? Annu. Rev. Microbiol. 69 (2015) 505–526.
[26] E.L. Mettert, P.J. Kiley, Fe-S proteins that regulate gene expression, Biochim. Biophys. Acta 2015 (1853) 1284–1293.
[27] D.M. Bodenmiller, S. Spiro, The *yjeB* (*nsrR*) gene of *Escherichia coli* encodes a nitric oxide-sensitive transcriptional regulator, J. Bacteriol. 188 (2006) 874–881.
[28] T.A. Rouault, The role of iron regulatory proteins in mammalian iron homeostasis and disease, Nat. Chem. Biol. 2 (2006) 406–414.
[29] A.J. Heck, Native mass spectrometry: a bridge between interactomics and structural biology, Nat. Methods 5 (2008) 927–933.
[30] A.C. Leney, A.J. Heck, Native mass spectrometry: what is in the name? J. Am. Soc. Mass Spectrom. 28 (2017) 5–13.
[31] D. Zhu, H. Su, C. Ke, C. Tang, M. Witt, R.J. Quinn, Y. Xu, J. Liu, Y. Ye, Efficient discovery of potential inhibitors for SARS-CoV-2 3C-like protease from herbal extracts using a native MS-based affinity-selection method, J. Pharm. Biomed. Anal. 209 (2022) 114538.
[32] S. Tamara, M.A. den Boer, A.J.R. Heck, High-resolution native mass spectrometry, Chem. Revs. 122 (2022) 7269–7326.
[33] A.F.M. Gavriilidou, K. Sokratous, H.Y. Yen, L. De Colibus, High-throughput native mass spectrometry screening in drug discovery, Front. Mol. Biosci. 9 (2022) 837901.
[34] S. Banerjee, S. Mazumdar, Electrospray ionization mass spectrometry: a technique to access the information beyond the molecular weight of the analyte, Int. J. Anal. Chem. 2012 (2012) 282574.
[35] N. Morgner, C.V. Robinson, Linking structural change with functional regulation-insights from mass spectrometry, Curr. Opin. Struct. Biol. 22 (2012) 44–51.
[36] J.T. Hopper, C.V. Robinson, Mass spectrometry quantifies protein interactions - from molecular chaperones to membrane porins, Angew. Chem. Int. Ed. 53 (2014) 14002–14015.
[37] N.G. Housden, J.T. Hopper, N. Lukoyanova, D. Rodriguez-Larrea, J.A. Wojdyla, A. Klein, R. Kaminska, H. Bayley, H.R. Saibil, C.V. Robinson, C. Kleanthous, Intrinsically disordered protein threads through the bacterial outer-membrane porin OmpF, Science 340 (2013) 1570–1574.
[38] F.D. Kondrat, G.R. Kowald, C.A. Scarff, J.H. Scrivens, C.A. Blindauer, Resolution of a paradox by native mass spectrometry: facile occupation of all four metal binding sites in the dimeric zinc sensor SmtB, Chem. Commun. 49 (2013) 813–815.
[39] J. Ross, T. Lambert, C. Piergentili, D. He, K.J. Waldron, C.L. Mackay, J. Marles-Wright, D.J. Clarke, Mass spectrometry reveals the assembly pathway of encapsulated ferritins and highlights a dynamic ferroxidase interface, Chem. Commun. 56 (2020) 3417–3420.
[40] J.S. Scheller, G.W. Irvine, M.J. Stillman, Unravelling the mechanistic details of metal binding to mammalian metallothioneins from stoichiometric, kinetic, and binding affinity data, Dalton Trans. 47 (2018) 3613–3637.
[41] D.B. Ott, A. Hartwig, M.J. Stillman, Competition between Al^{3+} and Fe^{3+} binding to human transferrin and toxicological implications: structural investigations using ultra-high resolution ESI MS and CD spectroscopy, Metallomics 11 (2019) 968–981.
[42] F. Lermyte, J. Everett, Y.P.Y. Lam, C.A. Wootton, J. Brooks, M.P. Barrow, N. D. Telling, P.J. Sadler, P.B. O'Connor, J.F. Collingwood, Metal ion binding to the amyloid beta monomer studied by native top-down FTICR mass spectrometry, J. Am. Soc. Mass Spectrom. 30 (2019) 2123–2134.
[43] M.A. Maniero, R.G. Wuilloud, E.A. Callegari, P.N. Smichowski, M.A. Fanelli, Metalloproteomics analysis in human mammary cell lines treated with inorganic mercury, J. Trace Elem. Med. Biol. 58 (2020) 126441.
[44] P.L. Hagedoorn, Microbial Metalloproteomics, Proteomes 3 (2015) 424–439.
[45] D.J. Hare, A. Rembach, B.R. Roberts, The emerging role of metalloproteomics in Alzheimer's disease research, Meth. Mol. Biol. 1303 (2016) 379–389.

[46] D.W. Woodall, C.J. Brown, S.A. Raab, T.J. El-Baba, A. Laganowsky, D.H. Russell, D.E. Clemmer, Melting of hemoglobin in native solutions as measured by IMS-MS, Anal. Chem. 92 (2020) 3440–3446.

[47] K.L. Kay, C.J. Hamilton, N.E. Le Brun, Mass spectrometric studies of Cu(I)-binding to the N-terminal domains of *B. subtilis* CopA and influence of bacillithiol, J. Inorg. Biochem. 190 (2019) 24–30.

[48] L. Zhou, K.L. Kay, O. Hecht, G.R. Moore, N.E. Le Brun, The N-terminal domains of *Bacillus subtilis* CopA do not form a stable complex in the absence of their inter-domain linker, Biochim. Biophys. Acta 2018 (1866) 275–282.

[49] S.P. Bennett, M.J. Soriano-Laguna, J.M. Bradley, D.A. Svistunenko, D. J. Richardson, A.J. Gates, N.E. Le Brun, NosL is a dedicated copper chaperone for assembly of the CuZ center of nitrous oxide reductase, Chem. Sci. 10 (2019) 4985–4993.

[50] J.M. Moulis, N. Scherrer, J. Gagnon, E. Forest, Y. Petillot, D. Garcia, Primary structure of *Chromatium tepidum* high-potential iron-sulfur protein in relation to thermal denaturation, Arch. Biochem. Biophys. 305 (1993) 186–192.

[51] Y. Petillot, E. Forest, J. Meyer, J.M. Moulis, Observation of holoprotein molecular ions of several ferredoxins by electrospray-ionization-mass spectrometry, Anal. Biochem. 228 (1995) 56–63.

[52] H. Hernandez, K.S. Hewitson, P. Roach, N.M. Shaw, J.E. Baldwin, C.V. Robinson, Observation of the iron-sulfur cluster in *Escherichia coli* biotin synthase by nanoflow electrospray mass spectrometry, Anal. Chem. 73 (2001) 4154–4161.

[53] K.A. Johnson, I.J. Amster, First observation by mass spectrometry of a 3+ oxidation state for a [4Fe-4S] metalloprotein: an ESI-FTICR mass spectrometry study of the high potential iron-sulfur protein from *Chromatium vinosum*, J. Am. Soc. Mass Spectrom. 12 (2001) 819–825.

[54] K.A. Johnson, M.F. Verhagen, P.S. Brereton, M.W. Adams, I.J. Amster, Probing the stoichiometry and oxidation states of metal centers in iron-sulfur proteins using electrospray FTICR mass spectrometry, Anal. Chem. 72 (2000) 1410–1418.

[55] J.C. Crack, A.A. Gaskell, J. Green, M.R. Cheesman, N.E. Le Brun, A.J. Thomson, Influence of the environment on the $[4Fe\text{-}4S]^{2+}$ to $[2Fe\text{-}2S]^{2+}$ cluster switch in the transcriptional regulator FNR, J. Am. Chem. Soc. 130 (2008) 1749–1758.

[56] J.C. Crack, J. Green, A.J. Thomson, N.E. Le Brun, Techniques for the production, isolation, and analysis of iron-sulfur proteins, Meth. Mol. Biol. 1122 (2014) 33–48.

[57] J.C. Crack, N.E. Le Brun, Native mass spectrometry of iron-sulfur proteins, Meth. Mol. Biol. 2353 (2021) 231–258.

[58] M.T. Pellicer Martinez, A.B. Martinez, J.C. Crack, J.D. Holmes, D.A. Svistunenko, A.W.B. Johnston, M.R. Cheesman, J.D. Todd, N.E. Le Brun, Sensing iron availability via the fragile [4Fe-4S] cluster of the bacterial transcriptional repressor RirA, Chem. Sci. 8 (2017) 8451–8463.

[59] S.A. Freibert, B.D. Weiler, E. Bill, A.J. Pierik, U. Muhlenhoff, R. Lill, Biochemical reconstitution and spectroscopic analysis of iron-sulfur proteins, Meth. Enzymol. 599 (2018) 197–226.

[60] S. Arakawa, T. Kimura, Preparation and partial characterization of iron-sulfur, iron-selenium, and iron-tellurium complexes of bovine serum albumin, Biochim. Biophys. Acta 580 (1979) 382–391.

[61] A. Laganowsky, E. Reading, J.T. Hopper, C.V. Robinson, Mass spectrometry of intact membrane protein complexes, Nat. Protoc. 8 (2013) 639–651.

[62] M. Barth, C. Schmidt, Native mass spectrometry-a valuable tool in structural biology, J. Mass Spectrom. 55 (2020) e4578.

[63] D. Lemaire, G. Marie, L. Serani, O. Laprevote, Stabilization of gas-phase noncovalent macromolecular complexes in electrospray mass spectrometry using aqueous triethylammonium bicarbonate buffer, Anal. Chem. 73 (2001) 1699–1706.

[64] J.B. Hedges, S. Vahidi, X. Yue, L. Konermann, Effects of ammonium bicarbonate on the electrospray mass spectra of proteins: evidence for bubble-induced unfolding, Anal. Chem. 85 (2013) 6469–6476.

[65] X. Zhuang, A.F.M. Gavriilidou, R. Zenobi, Influence of alkylammonium acetate buffers on protein-ligand noncovalent interactions using native mass spectrometry, J. Am. Soc. Mass Spectrom. 28 (2017) 341–346.

[66] M.M. Kostelic, M.T. Marty, Deconvolving native and intact protein mass spectra with UniDec, Meth. Mol. Biol. 2500 (2022) 159–180.

[67] J.C. Crack, A.J. Thomson, N.E. Le Brun, Mass spectrometric identification of intermediates in the O_2-driven [4Fe-4S] to [2Fe-2S] cluster conversion in FNR, Proc. Natl. Acad. Sci. U. S. A. 114 (2017) E3215–E3223.

[68] J.C. Crack, N. Le Brun, Mass spectrometric identification of $[4Fe\text{-}4S](NO)_x$ intermediates of nitric oxide sensing by regulatory iron-sulfur cluster proteins, Chemistry 25 (2019) 3675–3684.

[69] S.M.J.C. Crack, N.E. Le Brun, Generation of ^{34}S-substituted protein-bound [4Fe-4S] clusters using ^{34}S-L-cysteine, Biol. Meth. Prot. 4 (2019) byp015.

[70] M.T. Pellicer Martinez, J.C. Crack, M.Y. Stewart, J.M. Bradley, D.A. Svistunenko, A.W. Johnston, M.R. Cheesman, J.D. Todd, N.E. Le Brun, Mechanisms of iron- and O_2-sensing by the [4Fe-4S] cluster of the global iron regulator RirA, Elife 8 (2019) e47804.

[71] J.C. Crack, C.J. Hamilton, N.E. Le Brun, Mass spectrometric detection of iron nitrosyls, sulfide oxidation and mycothiolation during nitrosylation of the NO sensor [4Fe-4S] NsrR, Chem. Commun. 54 (2018) 5992–5995.

[72] D.W. Bak, E. Weerapana, Monitoring Fe-S cluster occupancy across the *E. coli* proteome using chemoproteomics, Nat. Chem. Biol. 19 (2023) 356–366.

[73] E. Gray, M.Y.Y. Stewart, L. Hanwell, J.C. Crack, R. Devine, C.E.M. Stevenson, A. Volbeda, A.W.B. Johnston, J.C. Fontecilla-Camps, M.I. Hutchings, J.D. Todd, N.E. Le Brun, Stabilisation of the RirA [4Fe-4S] cluster results in loss of iron-sensing function, Chem. Sci. 14 (2023) 9744–9758.

[74] P.J. Stephens, A.J. Thomson, J.B. Dunn, T.A. Keiderling, J. Rawlings, K.K. Rao, D. O. Hall, Circular dichroism and magnetic circular dichroism of iron-sulfur proteins, Biochemistry 17 (1978) 4770–4778.

[75] A. Volbeda, J.C. Crack, N.E. Le Brun, J.C. Fontecilla-Camps, Structure–function relationships of the NsrR and RsrR transcription regulators, in: Encyclopedia of Inorganic and Bioinorganic Chemistry, 2020, pp. 1–23.

[76] W. Shepard, O. Soutourina, E. Courtois, P. England, A. Haouz, I. Martin-Verstraete, Insights into the Rrf2 repressor family - the structure of CymR, the global cysteine regulator of *Bacillus subtilis*, FEBS J. 278 (2011) 2689–2701.

[77] J.T. Munnoch, M.T. Martinez, D.A. Svistunenko, J.C. Crack, N.E. Le Brun, M. I. Hutchings, Characterization of a putative NsrR homologue in *Streptomyces venezuelae* reveals a new member of the Rrf2 superfamily, Sci. Rep. 6 (2016) 31597.

[78] M.E. Belov, E. Damoc, E. Denisov, P.D. Compton, S. Horning, A.A. Makarov, N. L. Kelleher, From protein complexes to subunit backbone fragments: a multi-stage approach to native mass spectrometry, Anal. Chem. 85 (2013) 11163–11173.

[79] J.C. Crack, E. Gray, N.E. Le Brun, Sensing mechanisms of iron-sulfur cluster regulatory proteins elucidated using native mass spectrometry, Dalton Trans. 50 (2021) 7887–7897.

[80] J.C. Crack, P. Amara, A. Volbeda, J.M. Mouesca, R. Rohac, M.T. Pellicer Martinez, C.Y. Huang, O. Gigarel, C. Rinaldi, N.E. Le Brun, J.C. Fontecilla-Camps, Electron and proton transfers modulate DNA binding by the transcription regulator RsrR, J. Am. Chem. Soc. 142 (2020) 5104–5116.

[81] J.D. Mancias, X. Wang, S.P. Gygi, J.W. Harper, A.C. Kimmelman, Quantitative proteomics identifies NCOA4 as the cargo receptor mediating ferritinophagy, Nature 509 (2014) 105–109.

[82] T. Asano, M. Komatsu, Y. Yamaguchi-Iwai, F. Ishikawa, N. Mizushima, K. Iwai, Distinct mechanisms of ferritin delivery to lysosomes in iron-depleted and iron-replete cells, Mol. Cell. Biol. 31 (2011) 2040–2052.

[83] S. Kuno, K. Iwai, Oxygen modulates iron homeostasis by switching iron sensing of NCOA4, J. Biol. Chem. 299 (2023) 104701.

[84] J.D. Mancias, L. Pontano Vaites, S. Nissim, D.E. Biancur, A.J. Kim, X. Wang, Y. Liu, W. Goessling, A.C. Kimmelman, J.W. Harper, Ferritinophagy via NCOA4 is required for erythropoiesis and is regulated by iron dependent HERC2-mediated proteolysis, Elife 4 (2015) e10308.

[85] H. Zhao, Y. Lu, J. Zhang, Z. Sun, C. Cheng, Y. Liu, L. Wu, M. Zhang, W. He, S. Hao, K. Li, NCOA4 requires a [3Fe-4S] to sense and maintain the iron homeostasis, J. Biol. Chem. 300 (2023) 105612.

[86] R.N. Ledbetter, A.M. Garcia Costas, C.E. Lubner, D.W. Mulder, M. Tokmina-Lukaszewska, J.H. Artz, A. Patterson, T.S. Magnuson, Z.J. Jay, H.D. Duan, J. Miller, M.H. Plunkett, J.P. Hoben, B.M. Barney, R.P. Carlson, A.F. Miller, B. Bothner, P.W. King, J.W. Peters, L.C. Seefeldt, The electron bifurcating FixABCX protein complex from *Azotobacter vinelandii*: generation of low-potential reducing equivalents for nitrogenase catalysis, Biochemistry 56 (2017) 4177–4190.

[87] E. Krol, L. Werel, L.O. Essen, A. Becker, Structural and functional diversity of bacterial cyclic nucleotide perception by CRP proteins, Microlife 4 (2023) uqad024.

[88] M. Matsui, M. Tomita, A. Kanai, Comprehensive computational analysis of bacterial CRP/FNR superfamily and its target motifs reveals stepwise evolution of transcriptional networks, Genom. Biol. Evol. 5 (2013) 267–282.

[89] H. Komori, S. Inagaki, S. Yoshioka, S. Aono, Y. Higuchi, Crystal structure of CO-sensing transcription activator CooA bound to exogenous ligand imidazole, J. Mol. Biol. 367 (2007) 864–871.

[90] Y.Y. Lee, N. Shearer, S. Spiro, Transcription factor NNR from *Paracoccus denitrificans* is a sensor of both nitric oxide and oxygen: isolation of *nnr** alleles encoding effector-independent proteins and evidence for a haem-based sensing mechanism, Microbiology 152 (2006) 1461–1470.

[91] C. Scott, J.R. Guest, J. Green, Characterization of the *Lactococcus lactis* transcription factor FlpA and demonstration of an in vitro switch, Mol. Microbiol. 35 (2000) 1383–1393.

[92] S. Spiro, The FNR family of transcriptional regulators, Ant. Van Leeuwen. 66 (1994) 23–36.

[93] R.H. Holm, W. Lo, Structural conversions of synthetic and protein-bound iron-sulfur clusters, Chem. Rev. 116 (2016) 13685–13713.

[94] N. Khoroshilova, C. Popescu, E. Munck, H. Beinert, P.J. Kiley, Iron-sulfur cluster disassembly in the FNR protein of *Escherichia coli* by O_2: [4Fe-4S] to [2Fe-2S] conversion with loss of biological activity, Proc. Natl. Acad. Sci. U. S. A. 94 (1997) 6087–6092.

[95] C.V. Popescu, D.M. Bates, H. Beinert, E. Munck, P.J. Kiley, Mössbauer spectroscopy as a tool for the study of activation/inactivation of the transcription regulator FNR in whole cells of *Escherichia coli*, Proc. Natl. Acad. Sci. U. S. A. 95 (1998) 13431–13435.

[96] P.J. Kiley, H. Beinert, Oxygen sensing by the global regulator, FNR: the role of the iron-sulfur cluster, FEMS Microbiol.Rev. 22 (1998) 341–352.

[97] B.A. Lazazzera, H. Beinert, N. Khoroshilova, M.C. Kennedy, P.J. Kiley, DNA binding and dimerization of the Fe-S-containing FNR protein from *Escherichia coli* are regulated by oxygen, J.Biol. Chem. 271 (1996) 2762–2768.

[98] J. Crack, J. Green, A.J. Thomson, Mechanism of oxygen sensing by the bacterial transcription factor fumarate-nitrate reduction (FNR), J. Biol. Chem. 279 (2004) 9278–9286.

[99] J.C. Crack, J. Green, M.R. Cheesman, N.E. Le Brun, A.J. Thomson, Superoxide-mediated amplification of the oxygen-induced switch from [4Fe-4S] to [2Fe-2S] clusters in the transcriptional regulator FNR, Proc. Natl. Acad. Sci. U. S. A. 104 (2007) 2092–2097.

[100] A. Volbeda, C. Darnault, O. Renoux, Y. Nicolet, J.C. Fontecilla-Camps, The crystal structure of the global anaerobic transcriptional regulator FNR explains its extremely fine-tuned monomer-dimer equilibrium, Sci. Adv. 1 (2015) e1501086.
[101] P.J. Kiley, W.S. Reznikoff, Fnr mutants that activate gene expression in the presence of oxygen, J. Bacteriol. 173 (1991) 16–22.
[102] D.M. Bates, C.V. Popescu, N. Khoroshilova, K. Vogt, H. Beinert, E. Munck, P. J. Kiley, Substitution of leucine 28 with histidine in the *Escherichia coli* transcription factor FNR results in increased stability of the [4Fe-4S]$^{2+}$ cluster to oxygen, J. Biol. Chem. 275 (2000) 6234–6240.
[103] T. Overton, E.G. Reid, R. Foxall, H. Smith, S.J. Busby, J.A. Cole, Transcription activation at *Escherichia coli* FNR-dependent promoters by the gonococcal FNR protein: effects of a novel S18F substitution and comparisons with the corresponding substitution in *E. coli* FNR, J. Bacteriol. 185 (2003) 4734–4747.
[104] A.J. Jervis, J.C. Crack, G. White, P.J. Artymiuk, M.R. Cheesman, A.J. Thomson, N. E. Le Brun, J. Green, The O_2 sensitivity of the transcription factor FNR is controlled by Ser24 modulating the kinetics of [4Fe-4S] to [2Fe-2S] conversion, Proc. Natl. Acad. Sci. U. S. A. 106 (2009) 4659–4664.
[105] J.C. Crack, P. Amara, E. de Rosny, C. Darnault, M.R. Stapleton, J. Green, A. Volbeda, J.C. Fontecilla-Camps, N.E. Le Brun, Probing the reactivity of [4Fe-4S] fumarate and nitrate reduction (FNR) regulator with O_2 and NO: increased O_2 resistance and relative specificity for NO of the [4Fe-4S] L28H FNR cluster, Inorganics 11 (2023) 450.
[106] B.A. Lazazzera, D.M. Bates, P.J. Kiley, The activity of the *Escherichia coli* transcription factor FNR is regulated by a change in oligomeric state, Genes Dev. 7 (1993) 1993–2005.
[107] Y. Lee, I.-R. Jeon, K.A. Abboud, R. García-Serres, J. Shearer, L.J. Murray, A [3Fe–3S]$^{3+}$ cluster with exclusively μ-sulfide donors, Chem. Commun. 52 (2016) 1174–1177.
[108] E.L. Mettert, P.J. Kiley, Reassessing the structure and function relationship of the O_2 sensing transcription factor FNR, Antiox. Red. Sig. 29 (2018) 1830–1840.
[109] A. Volbeda, Y. Nicolet, J.C. Fontecilla-Camps, Fumarate and nitrate reduction regulator (FNR), encyclopedia of inorganic and bioinorganic, Chemistry (2017) 1–11.
[110] J.C. Crack, M.R. Stapleton, J. Green, A.J. Thomson, N.E. Le Brun, Mechanism of [4Fe-4S](Cys)$_4$ cluster nitrosylation is conserved among NO-responsive regulators, J. Biol. Chem. 288 (2013) 11492–11502.
[111] C.E. Vine, J.A. Cole, Unresolved sources, sinks, and pathways for the recovery of enteric bacteria from nitrosative stress, FEMS Microbiol. Lett. 325 (2011) 99–107.
[112] O. Chumsakul, D.P. Anantsri, T. Quirke, T. Oshima, K. Nakamura, S. Ishikawa, M. M. Nakano, Genome-wide analysis of ResD, NsrR, and Fur binding in *Bacillus subtilis* during anaerobic fermentative growth by *in vivo* footprinting, J. Bacteriol. 199 (2017) e00086-17.
[113] N. Filenko, S. Spiro, D.F. Browning, D. Squire, T.W. Overton, J. Cole, C. Constantinidou, The NsrR regulon of *Escherichia coli* K-12 includes genes encoding the hybrid cluster protein and the periplasmic, respiratory nitrite reductase, J. Bacteriol. 189 (2007) 4410–4417.
[114] K. Heurlier, M.J. Thomson, N. Aziz, J.W. Moir, The nitric oxide (NO)-sensing repressor NsrR of *Neisseria meningitidis* has a compact regulon of genes involved in NO synthesis and detoxification, J. Bacteriol. 190 (2008) 2488–2495.
[115] R.K. Poole, Flavohaemoglobin: the pre-eminent nitric oxide-detoxifying machine of microorganisms, F1000Res 9 (2020) 7.
[116] S. Honma, S. Ito, S. Yajima, Y. Sasaki, Nitric oxide signaling for actinorhodin production in *Streptomyces coelicolor* A3(2) via the DevS/R two-component system, Appl. Environ. Microbiol. 87 (2021) e0048021.
[117] S. Honma, S. Ito, S. Yajima, Y. Sasaki, Nitric oxide signaling for aerial mycelium formation in *Streptomyces coelicolor* A3(2) M145, Appl. Environ. Microbiol. 88 (2022) e0122222.
[118] Y. Sasaki, H. Oguchi, T. Kobayashi, S. Kusama, R. Sugiura, K. Moriya, T. Hirata, Y. Yukioka, N. Takaya, S. Yajima, S. Ito, K. Okada, K. Ohsawa, H. Ikeda, H. Takano, K. Ueda, H. Shoun, Nitrogen oxide cycle regulates nitric oxide levels and bacterial cell signaling, Sci. Rep. 6 (2016) 22038.
[119] N.P. Tucker, M.G. Hicks, T.A. Clarke, J.C. Crack, G. Chandra, N.E. Le Brun, R. Dixon, M.I. Hutchings, The transcriptional repressor protein NsrR senses nitric oxide directly via a [2Fe-2S] cluster, PloS One 3 (2008) e3623.
[120] N.P. Tucker, N.E. Le Brun, R. Dixon, M.I. Hutchings, There's NO stopping NsrR, a global regulator of the bacterial NO stress response, Trends Microbiol. 18 (2010) 149–156.
[121] E.T. Yukl, M.A. Elbaz, M.M. Nakano, P. Moenne-Loccoz, Transcription factor NsrR from *Bacillus subtilis* senses nitric oxide with a 4Fe-4S cluster, Biochemistry 47 (2008) 13084–13092.
[122] A. Volbeda, E.L. Dodd, C. Darnault, J.C. Crack, O. Renoux, M.I. Hutchings, N.E. Le Brun, J.C. Fontecilla-Camps, Crystal structures of the NO sensor NsrR reveal how its iron-sulfur cluster modulates DNA binding, Nat. Commun. 8 (2017) 15052.
[123] X. Duan, J. Yang, B. Ren, G. Tan, H. Ding, Reactivity of nitric oxide with the [4Fe-4S] cluster of dihydroxyacid dehydratase from *Escherichia coli*, Biochem. J. 417 (2009) 783–789.
[124] M.W. Foster, J.A. Cowan, Chemistry of nitric oxide with protein-bound iron sulfur centers. Insights on physiological reactivity, J. Am. Chem. Soc. 121 (1999) 4093–4100.
[125] J.C. Crack, L.J. Smith, M.R. Stapleton, J. Peck, N.J. Watmough, M.J. Buttner, R. S. Buxton, J. Green, V.S. Oganesyan, A.J. Thomson, N.E. Le Brun, Mechanistic insight into the nitrosylation of the [4Fe-4S] cluster of WhiB-like proteins, J. Am. Chem. Soc. 133 (2011) 1112–11121.
[126] A.R. Butler, C. Glidewell, M. Li, Nitrosyl complexes of iron-sulfur clusters, Adv. Inorg. Chem. 32 (1988) 335–393.
[127] Z.J. Tonzetich, H. Wang, D. Mitra, C.E. Tinberg, L.H. Do, F.E. Jenney Jr., M. W. Adams, S.P. Cramer, S.J. Lippard, Identification of protein-bound dinitrosyl iron complexes by nuclear resonance vibrational spectroscopy, J. Am. Chem. Soc. 132 (2010) 6914–6916.
[128] E. Victor, S.J. Lippard, A tetranitrosyl [4Fe-4S] cluster forms en route to Roussin's black anion: nitric oxide reactivity of [$Fe_4S_4(LS_3)L'$]$^{2-}$, Inorg. Chem. 53 (2014) 5311–5320.
[129] J.C. Crack, D.A. Svistunenko, J. Munnoch, A.J. Thomson, M.I. Hutchings, N.E. Le Brun, Differentiated, promoter-specific response of [4Fe-4S] NsrR DNA binding to reaction with nitric oxide, J. Biol. Chem. 291 (2016) 8663–8672.
[130] F. Wittkamp, N. Mishra, H. Wang, H.C. Wille, R. Steinbrugge, M. Kaupp, S. P. Cramer, U.P. Apfel, V. Pelmenschikov, Insights from ^{125}Te and ^{57}Fe nuclear resonance vibrational spectroscopy: a [4Fe-4Te] cluster from two points of view, Chem. Sci. 10 (2019) 7535–7541.
[131] P.N. Serrano, H. Wang, J.C. Crack, C. Prior, M.I. Hutchings, A.J. Thomson, S. Kamali, Y. Yoda, J. Zhao, M.Y. Hu, E.E. Alp, V.S. Oganesyan, N.E. Le Brun, S. P. Cramer, Nitrosylation of nitric oxide-sensing regulatory proteins containing [4Fe-4S] clusters gives rise to multiple iron-nitrosyl complexes, Angew. Chem. Int. Ed. 55 (2016) 14575–14579.
[132] L.K. Keefer, R.W. Nims, K.M. Davies, D.A. Wink, "NONOates" (1-substituted diazen-1-ium-1,2-diolates) as nitric oxide donors: convenient nitric oxide dosage forms, Meth. Enzymol. 268 (1996) 281–293.
[133] Y. Kim, A. Sridharan, D.L.M. Suess, The elusive mononitrosylated [Fe_4S_4] cluster in three redox states, Angew. Chem. Int. Ed. 61 (2022) e202213032.
[134] S.W. Yeh, C.C. Tsou, W.F. Liaw, The dinitrosyliron complex [$Fe_4(mu_3\text{-}S)_2(mu_2\text{-}NO)_2(NO)_6$]$^{2-}$ containing bridging nitroxyls: ^{15}N (NO) NMR analysis of the bridging and terminal NO-coordinate ligands, Dalton Trans. 43 (2014) 9022–9025.
[135] T.-N. Chen, F.-C. Lo, M.-L. Tsai, K.-N. Shih, M.-H. Chiang, G.-H. Lee, W.-F. Liaw, Dinitrosyl iron complexes [$E_5Fe(NO)_2$]$^-$ (E=S, se): a precursor of Roussin's black salt [$Fe_4E_3(NO)_7$]$^-$, Inorg. Chim. Acta 359 (2006) 2525–2533.
[136] R. Rohac, J.C. Crack, E. de Rosny, O. Gigarel, N.E. Le Brun, J.C. Fontecilla-Camps, A. Volbeda, Structural determinants of DNA recognition by the NO sensor NsrR and related Rrf2-type [FeS]-transcription factors, Commun. Biol. 5 (2022) 769.
[137] E. Fabiano, M.R. O'Brian, Mechanisms and regulation of iron homeostasis in the rhizobia, in: D. Expert, M.R. O'Brian (Eds.), Molecular Aspects of iron Metabolism in Pathogenic and Symbiotic Plant-Microbe Associations, Springer, Netherlands, Dordrecht, 2012, pp. 41–86.
[138] A.W. Johnston, J.D. Todd, A.R. Curson, S. Lei, N. Nikolaidou-Katsaridou, M. S. Gelfand, D.A. Rodionov, Living without Fur: the subtlety and complexity of iron-responsive gene regulation in the symbiotic bacterium *Rhizobium* and other alpha-proteobacteria, Biometals 20 (2007) 501–511.
[139] M. Behringer, L. Plotzky, D. Baabe, M.K. Zaretzke, P. Schweyen, M. Broring, D. Jahn, E. Hartig, RirA of *Dinoroseobacter shibae* senses iron via a [3Fe-4S]$^{1+}$ cluster co-ordinated by three cysteine residues, Biochem. J. 477 (2020) 191–212.
[140] D.A. Rodionov, M.S. Gelfand, J.D. Todd, A.R. Curson, A.W. Johnston, Computational reconstruction of iron- and manganese-responsive transcriptional networks in alpha-proteobacteria, PLoS Comp. Biol. 2 (2006) e163.
[141] M.J. Bush, The actinobacterial WhiB-like (Wbl) family of transcription factors, Mol. Microbiol. 110 (2018) 663–676.
[142] J. Rybniker, A. Nowag, E. van Gumpel, N. Nissen, N. Robinson, G. Plum, P. Hartmann, Insights into the function of the WhiB-like protein of mycobacteriophage TM4 - a transcriptional inhibitor of WhiB2, Mol. Microbiol. 77 (2010) 642–657.
[143] V. Sharma, A. Hardy, T. Luthe, J. Frunzke, Phylogenetic distribution of WhiB- and Lsr2-type regulators in actinobacteriophage genomes, Microbiol. Spectr. 9 (2021) e0072721.
[144] D.E. Geiman, T.R. Raghunand, N. Agarwal, W.R. Bishai, Differential gene expression in response to exposure to antimycobacterial agents and other stress conditions among seven *Mycobacterium tuberculosis whiB*-like genes, Antimicrob. Agents Chemother. 50 (2006) 2836–2841.
[145] J.C. Crack, C.D. den Hengst, P. Jakimowicz, S. Subramanian, M.K. Johnson, M. J. Buttner, A.J. Thomson, N.E. Le Brun, Characterization of [4Fe-4S]-containing and cluster-free forms of *Streptomyces* WhiD, Biochemistry 48 (2009) 12252–12264.
[146] P. Jakimowicz, M.R. Cheesman, W.R. Bishai, K.F. Chater, A.J. Thomson, M. J. Buttner, Evidence that the *Streptomyces* developmental protein WhiD, a member of the WhiB family, binds a [4Fe-4S] cluster, J. Biol. Chem. 280 (2005) 8309–8315.
[147] B.K. Kudhair, A.M. Hounslow, M.D. Rolfe, J.C. Crack, D.M. Hunt, R.S. Buxton, L. J. Smith, N.E. Le Brun, M.P. Williamson, J. Green, Structure of a Wbl protein and implications for NO sensing by *M. tuberculosis*, Nat. Commun. 8 (2017) 2280.
[148] M. Lilic, N.A. Holmes, M.J. Bush, A.K. Marti, D.A. Widdick, K.C. Findlay, Y. J. Choi, R. Froom, S. Koh, M.J. Buttner, E.A. Campbell, Structural basis of dual activation of cell division by the actinobacterial transcription factors WhiA and WhiB, Proc. Natl. Acad. Sci. U. S. A. 120 (2023) e2220785120.
[149] A. Singh, L. Guidry, K.V. Narasimhulu, D. Mai, J. Trombley, K.E. Redding, G. I. Giles, J.R. Lancaster Jr., A.J. Steyn, *Mycobacterium tuberculosis* WhiB3 responds to O_2 and nitric oxide via its [4Fe-4S] cluster and is essential for nutrient starvation survival, Proc. Natl. Acad. Sci. U. S. A. 104 (2007) 11562–11567.
[150] L.J. Smith, M.R. Stapleton, G.J. Fullstone, J.C. Crack, A.J. Thomson, N.E. Le Brun, D.M. Hunt, E. Harvey, S. Adinolfi, R.S. Buxton, J. Green, *Mycobacterium tuberculosis* WhiB1 is an essential DNA-binding protein with a nitric oxide-sensitive iron-sulfur cluster, Biochem. J. 432 (2010) 417–427.

[151] M.Y.Y. Stewart, M.J. Bush, J.C. Crack, M.J. Buttner, N.E. Le Brun, Interaction of the *Streptomyces* Wbl protein WhiD with the principal sigma factor sigma(HrdB) depends on the WhiD [4Fe-4S] cluster, J. Biol. Chem. 295 (2020) 9752–9765.
[152] T. Wan, M. Horova, D.G. Beltran, S. Li, H.X. Wong, L.M. Zhang, Structural insights into the functional divergence of WhiB-like proteins in *Mycobacterium tuberculosis*, Mol. Cell 81 (2021) 2887–2900 e5.
[153] T. Wan, M. Horova, V. Khetrapal, S. Li, C. Jones, A. Schacht, X. Sun, L. Zhang, Structural basis of DNA binding by the WhiB-like transcription factor WhiB3 in *Mycobacterium tuberculosis*, J. Biol. Chem. 299 (2023) 104777.
[154] T. Wan, S. Li, D.G. Beltran, A. Schacht, L. Zhang, D.F. Becker, L. Zhang, Structural basis of non-canonical transcriptional regulation by the sigmaA-bound iron-sulfur protein WhiB1 in *M. tuberculosis*, Nucl. Acids Res. 48 (2020) 501–516.
[155] R.P. Morris, L. Nguyen, J. Gatfield, K. Visconti, K. Nguyen, D. Schnappinger, S. Ehrt, Y. Liu, L. Heifets, J. Pieters, G. Schoolnik, C.J. Thompson, Ancestral antibiotic resistance in *Mycobacterium tuberculosis*, Proc. Natl. Acad. Sci. U. S. A. 102 (2005) 12200–12205.
[156] M.R. Stapleton, L.J. Smith, D.M. Hunt, R.S. Buxton, J. Green, *Mycobacterium tuberculosis* WhiB1 represses transcription of the essential chaperonin GroEL2, Tuberculosis 92 (2012) 328–332.
[157] V. Saini, A. Farhana, A.J. Steyn, *Mycobacterium tuberculosis* WhiB3: a novel iron-sulfur cluster protein that regulates redox homeostasis and virulence, Antiox. Redox Sig. 16 (2012) 687–697.
[158] M. Lilic, S.A. Darst, E.A. Campbell, Structural basis of transcriptional activation by the *Mycobacterium tuberculosis* intrinsic antibiotic-resistance transcription factor WhiB7, Mol. Cell 81 (2021) 2875–2886 e5.
[159] K. Esquilin-Lebron, S. Dubrac, F. Barras, J.M. Boyd, Bacterial approaches for assembling iron-sulfur proteins, mBio 12 (2021) e0242521.
[160] R. Lill, From the discovery to molecular understanding of cellular iron-sulfur protein biogenesis, Biol. Chem. 401 (2020) 855–876.
[161] F. Barras, L. Loiseau, B. Py, How *Escherichia coli* and *Saccharomyces cerevisiae* build Fe/S proteins, Adv. Microb. Physiol. 50 (2005) 41–101.
[162] M. Blahut, E. Sanchez, C.E. Fisher, F.W. Outten, Fe-S cluster biogenesis by the bacterial Suf pathway, Biochim. Biophys. Acta 1867 (2020) 118829.
[163] P.S. Garcia, F. D'Angelo, S. Ollagnier de Choudens, M. Dussouchaud, E. Bouveret, S. Gribaldo, F. Barras, An early origin of iron-sulfur cluster biosynthesis machineries before earth oxygenation, Nat. Ecol. Evol. 6 (2022) 1564–1572.
[164] N. Tanaka, M. Kanazawa, K. Tonosaki, N. Yokoyama, T. Kuzuyama, Y. Takahashi, Novel features of the ISC machinery revealed by characterization of *Escherichia coli* mutants that survive without iron-sulfur clusters, Mol. Microbiol. 99 (2016) 835–848.
[165] J.W. Olson, J.N. Agar, M.K. Johnson, R.J. Maier, Characterization of the NifU and NifS Fe-S cluster formation proteins essential for viability in *Helicobacter pylori*, Biochemistry 39 (2000) 16213–16219.
[166] J.R. Cupp-Vickery, H. Urbina, L.E. Vickery, Crystal structure of IscS, a cysteine desulfurase from *Escherichia coli*, J. Mol. Biol. 330 (2003) 1049–1059.
[167] J.H. Kim, M. Tonelli, T. Kim, J.L. Markley, Three-dimensional structure and determinants of stability of the iron-sulfur cluster scaffold protein IscU from *Escherichia coli*, Biochemistry 51 (2012) 5557–5563.
[168] E.N. Marinoni, J.S. de Oliveira, Y. Nicolet, E.C. Raulfs, P. Amara, D.R. Dean, J. C. Fontecilla-Camps, $(IscS\text{-}IscU)_2$ complex structures provide insights into Fe_2S_2 biogenesis and transfer, Angew. Chem. Int. Ed. 51 (2012) 5439–5442.
[169] R. Shi, A. Proteau, M. Villarroya, I. Moukadiri, L. Zhang, J.F. Trempe, A. Matte, M.E. Armengod, M. Cygler, Structural basis for Fe-S cluster assembly and tRNA thiolation mediated by IscS protein-protein interactions, PLoS Biol. 8 (2010) e1000354.
[170] J.U. Dahl, C. Radon, M. Buhning, M. Nimtz, L.I. Leichert, Y. Denis, C. Jourlin-Castelli, C. Iobbi-Nivol, V. Mejean, S. Leimkuhler, The sulfur carrier protein TusA has a pleiotropic role in *Escherichia coli* that also affects molybdenum cofactor biosynthesis, J. Biol. Chem. 288 (2013) 5426–5442.
[171] S. Adinolfi, R. Puglisi, J.C. Crack, C. Iannuzzi, F. Dal Piaz, P.V. Konarev, D. I. Svergun, S. Martin, N.E. Le Brun, A. Pastore, The molecular bases of the dual regulation of bacterial iron-sulfur cluster biogenesis by CyaY and IscX, Front. Mol. Biosci. 4 (2017) 97.
[172] J.H. Kim, R.O. Frederick, N.M. Reinen, A.T. Troupis, J.L. Markley, [2Fe-2S]-ferredoxin binds directly to cysteine desulfurase and supplies an electron for iron-sulfur cluster assembly but is displaced by the scaffold protein or bacterial frataxin, J. Am. Chem. Soc. 135 (2013) 8117–8120.
[173] R. Puglisi, E. Boeri Erba, A. Pastore, A guide to native mass spectrometry to determine complex interactomes of molecular machines, FEBS J. 287 (2020) 2428–2439.
[174] S.P. Bennett, J.C. Crack, R. Puglisi, A. Pastore, N.E. Le Brun, Native mass spectrometric studies of IscSU reveal a concerted, sulfur-initiated mechanism of iron-sulfur cluster assembly, Chem. Sci. 14 (2022) 78–95.
[175] C.W. Lin, J.W. McCabe, D.H. Russell, D.P. Barondeau, Molecular mechanism of ISC iron-sulfur cluster biogenesis revealed by high-resolution native mass spectrometry, J. Am. Chem. Soc. 142 (2020) 6018–6029.
[176] D. di Maio, B. Chandramouli, R. Yan, G. Brancato, A. Pastore, Understanding the role of dynamics in the iron sulfur cluster molecular machine, Biochim. Biophys. Acta 2017 (1861) 3154–3163.
[177] S. Sato, Y. Matsushima, M. Kanazawa, N. Tanaka, T. Fujishiro, K. Kunichika, R. Nakamura, H. Tomioka, K. Wada, Y. Takahashi, Evidence for dynamic *in vivo* interconversion of the conformational states of IscU during iron-sulfur cluster biosynthesis, Mol. Microbiol. 115 (2021) 807–818.
[178] C. Iannuzzi, M. Adrover, R. Puglisi, R. Yan, P.A. Temussi, A. Pastore, The role of zinc in the stability of the marginally stable IscU scaffold protein, Prot. Sci. 23 (2014) 1208–1219.
[179] C.W. Lin, S.D. Oney-Hawthorne, S.T. Kuo, D.P. Barondeau, D.H. Russell, Mechanistic insights into IscU conformation regulation for Fe-S cluster biogenesis revealed by variable temperature electrospray ionization native ion mobility mass spectrometry, Biochemistry 61 (2022) 2733–2741.
[180] I. Elchennawi, P. Carpentier, C. Caux, M. Ponge, S. Ollagnier de Choudens, Structural and biochemical characterization of *Mycobacterium tuberculosis* zinc SufU-SufS complex, Biomolecules 13 (2023) 732.
[181] M. Jia, S. Sen, C. Wachnowsky, I. Fidai, J.A. Cowan, V.H. Wysocki, Characterization of [2Fe-2S]-cluster-bridged protein complexes and reaction intermediates by use of native mass spectrometric methods, Angew. Chem. Int. Ed. 59 (2020) 6724–6728.
[182] E. Weerapana, A.E. Speers, B.F. Cravatt, Tandem orthogonal proteolysis-activity-based protein profiling (TOP-ABPP) - a general method for mapping sites of probe modification in proteomes, Nat. Protoc. 2 (2007) 1414–1425.
[183] E. Weerapana, C. Wang, G.M. Simon, F. Richter, S. Khare, M.B. Dillon, D. A. Bachovchin, K. Mowen, D. Baker, B.F. Cravatt, Quantitative reactivity profiling predicts functional cysteines in proteomes, Nature 468 (2010) 790–795.
[184] S. Gervason, D. Larkem, A.B. Mansour, T. Botzanowski, C.S. Muller, L. Pecqueur, G. Le Pavec, A. Delaunay-Moisan, O. Brun, J. Agramunt, A. Grandas, M. Fontecave, V. Schunemann, S. Cianferani, C. Sizun, M.B. Toledano, B. D'Autreaux, Physiologically relevant reconstitution of iron-sulfur cluster biosynthesis uncovers persulfide-processing functions of ferredoxin-2 and frataxin, Nat. Commun. 10 (2019) 3566.
[185] A. Parent, X. Elduque, D. Cornu, L. Belot, J.P. Le Caer, A. Grandas, M.B. Toledano, B. D'Autreaux, Mammalian frataxin directly enhances sulfur transfer of NFS1 persulfide to both ISCU and free thiols, Nat. Commun. 6 (2015) 5686.
[186] B. Srour, S. Gervason, M.H. Hoock, B. Monfort, K. Want, D. Larkem, N. Trabelsi, G. Landrot, A. Zitolo, E. Fonda, E. Etienne, G. Gerbaud, C.S. Muller, J. Oltmanns, J.B. Gordon, V. Yadav, M. Kleczewska, M. Jelen, M.B. Toledano, R. Dutkiewicz, D. P. Goldberg, V. Schunemann, B. Guigliarelli, B. Burlat, C. Sizun, B. D'Autreaux, Iron insertion at the assembly site of the ISCU scaffold protein is a conserved process initiating Fe-S cluster biosynthesis, J. Am. Chem. Soc. 144 (2022) 17496–17515.
[187] J.C. May, J.A. McLean, Ion mobility-mass spectrometry: time-dispersive instrumentation, Anal. Chem. 87 (2015) 1422–1436.
[188] S. Vimer, G. Ben-Nissan, M. Sharon, Mass spectrometry analysis of intact proteins from crude samples, Anal. Chem. 92 (2020) 12741–12749.
[189] S. Vimer, G. Ben-Nissan, M. Sharon, Direct characterization of overproduced proteins by native mass spectrometry, Nat. Protoc. 15 (2020) 236–265.
[190] W. Sakamoto, N. Azegami, T. Konuma, S. Akashi, Single-cell native mass spectrometry of human erythrocytes, Anal. Chem. 93 (2021) 6583–6588.